MADITRACE

Methodology for on-site material flow characterization

Deliverable D2.3

Version N°2

Authors: Anne-Marie Desaulty (BRGM), Waltteri Alatalo (Metso), Robert Arato (MUL), Claire Aupart (BRGM), Nathan Bodereau (BRGM), Alban Moradell Casellas (BRGM), Gabriella Obbagy-Arato (MUL), Yuan Shang (GTK), Teemu Soini (Metso), Daniel Virokannas (Metso)

Funded by the European Union

Disclaimer

The content of this report reflects only the author's view. The European Commission is not responsible for any use that may be made of the information it contains.

Funded by
the European Union

Document information

Grant Agreement	n°101091502
Project Title	Material and digital traceability for the certification of critical raw materials
Project Acronym	MaDiTraCe
Project Coordinator	Daniel Monfort, BRGM
Project Duration	1 January 2023 – 30 June 2026 (42 months)
Related Work Package	WP2
Related Task(s)	T2.1 : On-site on-line MFP techniques
Lead Organisation	BRGM
Contributing Partner(s)	MUL, Metso, GTK
Due Date	28 February 2026
Submission Date	21 April 2026
Dissemination level	Public report, BRGM/RP-75373-FR

History

Date	Version	Submitted by	Reviewed by	Comments
30/03/2026	1	AM. Desaulty	Daniel Monfort	
07/04/2026	2	AM. Desaulty	Wolfram Kloppmann	
21/04/2026	Final	AM. Desaulty	Laurine Duivon/ Adeline Paul	

Funded by the European Union

Table of contents

Funded by the European Union

List of figures

Funded by the European Union

Funded by the European Union

List of tables

Funded by the European Union

Funded by
the European Union

Summary

This deliverable (D2.3) is part of the MaDiTraCe project, which aims to develop innovative approaches for the traceability and certification of critical raw materials along complex value chains. Within this framework, ensuring reliable and operational traceability requires the ability to characterize material flows directly on-site, at different stages of the production chain. This deliverable therefore focuses on the development of a methodology for on-site material flow characterization, as a key component of the overall traceability strategy of the project.

The main objective of this work is to identify, evaluate, and compare analytical techniques capable of generating relevant material fingerprints under industrial conditions. To achieve this, a harmonized evaluation framework was developed based on five criteria: mobility, production chain coverage, differentiating power, cost of implementation, and operational efficiency. These criteria were combined into a Global MFP Technic Index (GMTI), allowing for a quantitative and comparative assessment of the different techniques tested within the project.

The methodology was applied to two representative case studies: lithium and natural graphite, both critical raw materials used in battery production. For each value chain, key traceability points ("leverage points") were identified, corresponding to stages where material origin verification is most relevant. A selection of analytical techniques was then tested, including on-line and mobile LIBS, portable and mobile XRF, and mineral luminescence-based methods (UV bench and cathodoluminescence).

The results demonstrate that several of these techniques are capable of capturing geochemical signatures that can be used to discriminate the origin of materials, particularly when combined with multivariate data analysis and machine learning approaches. However, the performance of these techniques is influenced by operational conditions, sample characteristics, and measurement variability, requiring appropriate calibration strategies and data processing workflows.

The study also highlights that mobile analytical techniques are currently most effective for upstream stages of the value chain (raw materials and concentrates), while their applicability to downstream products remains limited. This underlines the need for complementary approaches to ensure full traceability across all processing stages.

Overall, this deliverable provides a structured and operational methodology for selecting and deploying analytical techniques for on-site material flow characterization. It contributes to the broader objectives of the MaDiTraCe project by supporting the development of reliable, scalable, and industry-compatible traceability systems for critical raw materials.

Funded by the European Union

Keywords

Chemical analysis, Material fingerprint, critical raw materials, geochemistry, traceability, machine learning, lithium, natural graphite

Abbreviations and acronyms

Acronym	Description
WP	Work Package
MFP	Material Fingerprinting
GMTI	Global MFP Technic Index
LIBS	Laser-Induced Breakdown Spectroscopy
µLIBS	Micro Laser-Induced Breakdown Spectroscopy
XRF	X-ray Fluorescence
ED-XRF	Energy Dispersive X-ray Fluorescence
PCA	Principal Component Analysis
DoE	Design of Experiments
AE	Autoencoder
RF	Random Forest
CAM	Cathode Active Material
LiOH	Lithium Hydroxide
NIR	Near Infrared
INAA	Neutron Activation Analysis
ICP-MS	Inductively Coupled Plasma Mass Spectrometry
LOO-CV	Leave-One-Out Cross-Validation
OvR	one-vs-rest

Funded by the European Union

1 Introduction

Within the framework of the MaDiTraCe project (Material and digital traceability for the certification of critical raw materials), ensuring the traceability of mineral resources along complex value chains is addressed as a key methodological and operational challenge. MaDiTraCe aims to develop and evaluate innovative approaches to enable reliable traceability across the different stages of production.

In this context, on-site material flow characterization represents a key component for verifying both the origin and integrity of materials, particularly in complex production systems such as lithium-ion battery supply chains. These value chains involve multiple processing steps and international transfers, making it difficult to track materials from extraction to final products.

This Deliverable D2.3, developed under WP2, aims to establish a robust methodology for on-site material flow characterization, with a particular focus on analytical techniques that can be deployed in industrial environments (e.g. On line LIBS, Handheld XRF, etc.). The objective is to identify, assess, and compare different methods capable of generating analytical signatures suitable for material traceability.

To this end, a harmonized set of criteria, including mobility, production chain coverage, differentiating power, cost of implementation, and operational efficiency were defined. These criteria are combined into a Global MFP Technic Index (GMTI), enabling an objective comparison of methods and supporting their selection for practical applications.

Finally, the proposed methodology is applied to specific case studies, notably lithium and natural graphite, which are key materials in battery manufacturing. The analysis focuses on identifying critical traceability points along the value chain and assessing the ability of selected techniques to provide reliable and actionable information in an industrial context. Due to the current scope of experimental work, only lithium and natural graphite are presented in this deliverable, as mobile analytical techniques were not tested along the cobalt and neodymium value chains.

Funded by
the European Union

2 Method evaluation

Within the framework of the MADITRACE project, a wide range of analytical techniques in the various laboratories were tested to develop traceability for the various commodities. Each technique was evaluated against a set of criteria, and a Global MFP Technic Index was also established.

2.1 Assessment criteria

Each analytical technique is evaluated against five criteria: mobility (M), production chain coverage (PCC), differentiating power (DP), cost of implementation (COI) and operational efficiency (OE). Each criterion scored from 0 (poor) to 10 (excellent) (Figure 1).

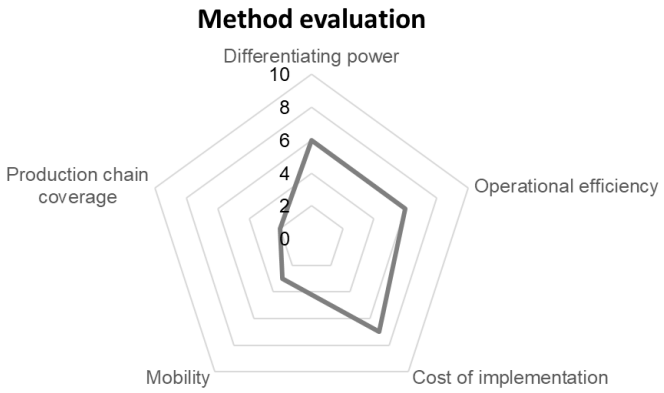

Figure 1: Example of method evaluation using the various criteria defined in this paragraph.

- **Mobility (M)** reflects the ease with which an analytical technique can be deployed outside a conventional laboratory environment. It accounts for the level of mobility (weight, size), infrastructure requirements (power supply, environmental control), and the degree of installation needed to perform analyses in the field or at production sites.

Score	Description	Examples
10	Fully mobile, handheld, battery-powered	Handheld XRF, handheld LIBS
8	Transportable but requires mains power	Mobile EDXRF
6	Transportable requires mains power and controlled environment	Cathodoluminescence
4	Semi-mobile (transport truck) requiring a dedicated room and fixed installation, but not a permanent laboratory	Movable µ-LIBS
0	Fixed laboratory technique	MC-ICP-MS

Funded by the European Union

- **Production Chain Coverage (PCC)** evaluates the extent to which an analytical technique can be applied across successive stages of the commodity production chain. It evaluates the ability of a method to analyse materials from primary resources through intermediate processing steps to final products, thereby enabling continuity of traceability along the production chain.

Score	Description
10	Entire chain (ore → concentrate → chemicals → product)
8-6	Most of the chain, but with limitations at some stages
4	Few stages only
2	One stage only (e.g. ore → concentrate)
0	Only one type of sample

- **Differentiating power (DP)** reflects the ability of an analytical technique to discriminate between different deposits or material origins and to correctly assign unknown samples. This criterion is assessed based on classification performance, including separation efficiency between groups and correct assignment or prediction success rates.

Score	Description
10	Excellent discrimination; high correct assignment rate
8-6	Good discrimination with some overlap
4	Moderate discrimination
2	Poor discrimination capability
0	No discrimination capability

- **Cost of implementation (COI)** reflects the overall financial requirements associated with deploying an analytical technique. It includes the instrument purchase price as well as implementation and operational costs, such as sample preparation and per-analysis expenses. Techniques that are already commonly available and deployed within the mining and extractive industry are expected to score more favorably, as their integration typically requires lower additional investment and operational adaptation.

Score	Description (device cost and sample cost)
10	< 50 k €, no expensive preparation
8	Between 50 k € and 100 k €, no expensive preparation
6	> 100 k €, no expensive preparation
4	> 100 k €, expensive preparation required
2	> 500 k €
0	> 500 k € with expensive and complex preparation

Funded by the European Union

- **Operational efficiency (OE):** This criterion combines analysis speed, preparation requirements, and operational constraints. The factors considered are: analysis time per sample, sample preparation complexity (requiring additional preparation time), safety constraints (X-rays, lasers, acids, etc.), need for operator certification or special authorization.

Score	Description
10	Very fast, minimal preparation, no special safety requirements
8-6	Moderate preparation and/or safety measures
4	Slow analysis or significant preparation
2	Slow analysis and significant preparation
0	Very slow, complex preparation, strict safety constraints

2.2 Global MFP Technic Index (GMTI)

The Global MFP Technic Index (GMTI) is a weighted composite score (0–10) that reflects the overall suitability of an analytical technique for traceability across the value chain.

The GMTI is defined as:

$$\mathbf{GMTI} = w_M M + w_{PCC} PCC + w_{DP} DP + w_{COI} COI + w_{OE} OE$$

with:

$$w_M + w_{PCC} + w_{DP} + w_{COI} + w_{OE} = 1$$

- M (mobility), PCC (production chain coverage), DP (differentiating power), COI (cost of implementation) and OE (operational efficiency) are the scores (0-10) for the criteria defined above.

- w_M, w_{PCC}, w_{DP}, w_{COI} and w_{OE} are the weights of the various criteria reflecting their priority

We conducted a survey among WP2 MADITRACE members to determine the relative weighting of the different criteria (n = 17). The survey results are presented in Figure 2. The median value was calculated for each criterion based on the voting results (Table 1). For traceability purposes, the ability of a method to discriminate origin (differentiating power) was identified as the most important criterion, with a weight of 0.30. The remaining criteria—production chain coverage, operational efficiency, and cost of implementation—were assigned equal weights of 0.20. Mobility received the lowest weight, with a value of 0.10.

Funded by the European Union

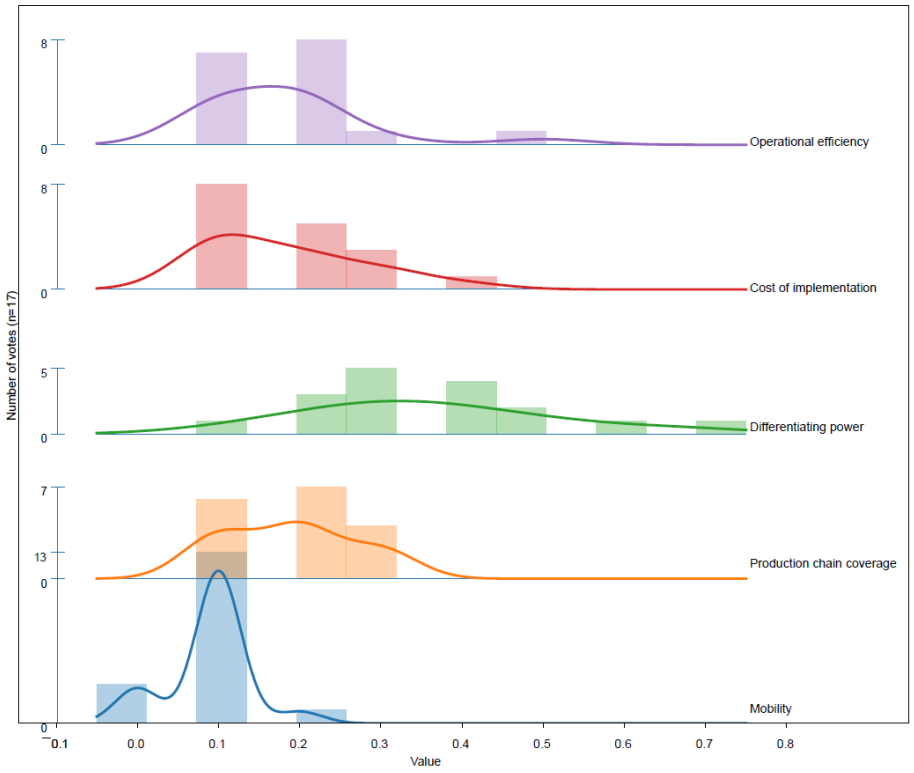

Figure 2 : Results of the survey for the weighting of the technic criteria (n=17).

Table 1: Weighting of the various criteria.

Criterion	Weight (**w**)	Justification
DP (Differentiating power)	0.30	Core requirement for provenance assignment
PCC (production chain coverage)	0.20	Essential to ensure continuity of traceability
M (Mobility)	0.10	Important for field control, but not decisive alone
OE (operational efficiency)	0.20	Key for operational deployment and scaling
COI (cost of implementation)	0.20	Important but secondary for strategic traceability

Funded by the European Union

3 Methodology for on-site material flow characterization along the battery production chain: lithium

3.1 Leverage points

There are several key points along the battery production chain (leverage point) where it is necessary to verify the origin of lithium. These key points are associated with changes in ownership or the transportation of the material (D3.8, Figure 3).

For hard rock sources, if mineral concentration takes place close to the mine, the mine concentrates can then be shipped to another country for lithium salt refining (for example, Australia → China).

For salars, if refining is carried out near the extraction site, battery-grade lithium salt production may take place in another country (e.g., Chile → China).

The production of cathode active material (e.g., CAM) may also occur in a different country (China → Japan), as well as battery manufacturing (e.g., Japan → China) and final assembly into the end product (e.g., China → France).

To implement a traceability system based on material fingerprinting (MFP), it is therefore necessary to identify parameters that can be monitored in the following samples:

- Ore concentrate
- Intermediate-grade lithium salt
- Battery-grade lithium salt
- Cathode active material (CAM)
- Cathode sheet or battery cell
- Battery integrated into the final product

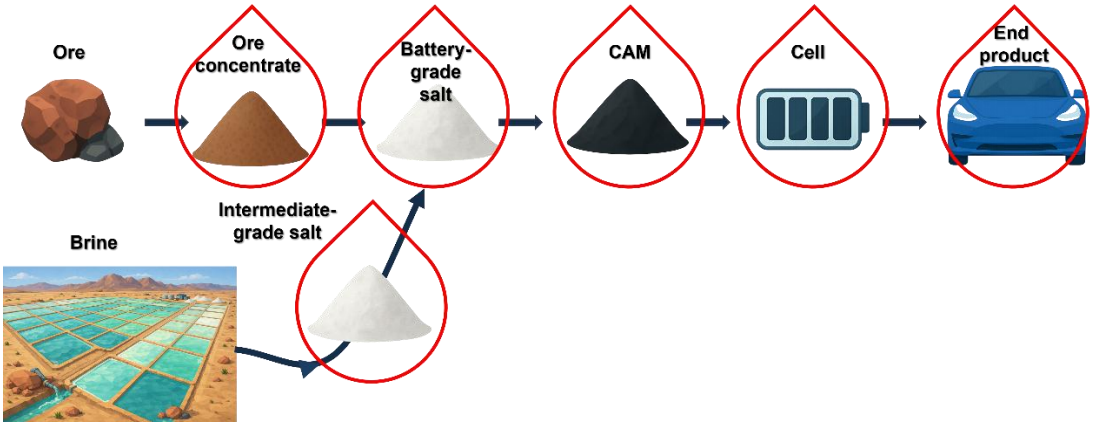

Figure 3: Key traceability points (leverage points) along the lithium battery value chain.

3.2 Selected techniques

Several mobile, field-deployable techniques were tested for the lithium traceability during the MADITRACE project (combined XRF-XRD, portable VNIR/SWIR, etc.). Ultimately, the following techniques were selected: on-line LIBS, mobile µLIBS, handheld XRF, benchtop EDXRF, cathodoluminescence, and UV bench.

3.2.1 Methods based on Laser Induced Breakdown Spectroscopy (LIBS): on-line LIBS and mobile µLIBS

Laser-induced breakdown spectroscopy (LIBS) is a method of atomic emission spectroscopy in which a focused, low-energy pulsed laser ablates a small mass of the target material and forms a transient microplasma. As the plasma cools, the constituent atoms and ions emit photons at element-specific wavelengths, producing a broadband emission spectrum that encodes the sample's elemental composition (Cremers & Radziemski, 2013, p. 69).

3.2.1.1 Online LIBS

- **Instruments description**

Measurements in this study were acquired using Metso Courier® 8X SL, a LIBS-based on-stream process analyser system for continuous elemental measurement of mineral slurries (Figure 4). The analyser employs a diode-pumped solid-state Nd:YAG laser and an echelle spectrometer coupled to an electron-multiplying charge-coupled device (EMCCD) detector, capable of distinguishing emission lines 0.1 nm apart. Each measurement produces a broadband emission spectrum spanning the ultraviolet to near-infrared range, capturing emission lines from all major rock-forming elements, as well as trace constituents relevant to provenance. Prior application feasibility studies using Courier 8X SL have confirmed that the analyzer's spectral response is sensitive to matrix variation between sample streams of differing composition (Köresaar, 2016).

Funded by the European Union

Figure 4: Metso Courier® 8X SL online LIBS system. Illustration includes the measurement probe and its accessories, and the online sampling system connected to it (top).

- **Method**

The elemental composition of a spodumene sample is governed by the geochemistry of its source deposit. Transition and post-transition metals such as Fe, Mn, Ga, and Sn substitute into the spodumene crystal lattice at concentrations that vary systematically with formation conditions. Principal component analysis of these trace elements has been shown to discriminate spodumene of different origins (Brennan et al., 2024). The broadband emission spectrum acquired by LIBS captures both major and trace element signatures simultaneously, making it possible to treat the full spectrum as a high-dimensional feature vector for multivariate provenance classification.

The goal of this study was to establish whether a provenance signal can be extracted from slurry-based LIBS measurements acquired using a Metso Courier® 8X SL process analyzer. The methodology covers two distinct tracks: a conventional methodology attempting to establish whether a provenance fingerprint exists in the dataset, and a deep learning methodology exploring the application of autoencoders to high-dimensional LIBS spectra.

- **Samples**

Two data sources were used in this study: i) spectra from customer feasibility studies from ten origin facilities, and ii) a 3x3 designed experiment (DoE) varying the instrument's gate delay and laser energy across seven measured samples from three customers. The samples consist of spodumene-mearing materials from different origins. All data was in the form of LIBS spectra.

- **Results**

Exploratory analysis

For the purposes of this analysis, spectra were baseline-corrected using SNIP (statistics-sensitive non-linear Iterative peak-clipping) and linearly resampled onto a shared

wavelength axis. Emission lines were integrated using a conventional trapezoidal, centered symmetrically ±1 nm around the peak center.

The DoE dataset comprises seven anonymized spodumene-bearing samples from distinct origins, each measured at all nine delay-energy combinations. Principal component analysis (PCA) showed that the dominant spectral variation is measurement state, specifically plasma temperature and atmospheric coupling, rather than material identity. PC1 captures 82 % of variance and aligns strongly with gate delay. The DoE also reveals that not all spectral features respond equally. Atmospheric and NIR lines track the shared plasma state, while a separate set of chemistry-bearing lines remains stable across instrument settings and retains material information (Figure 5).

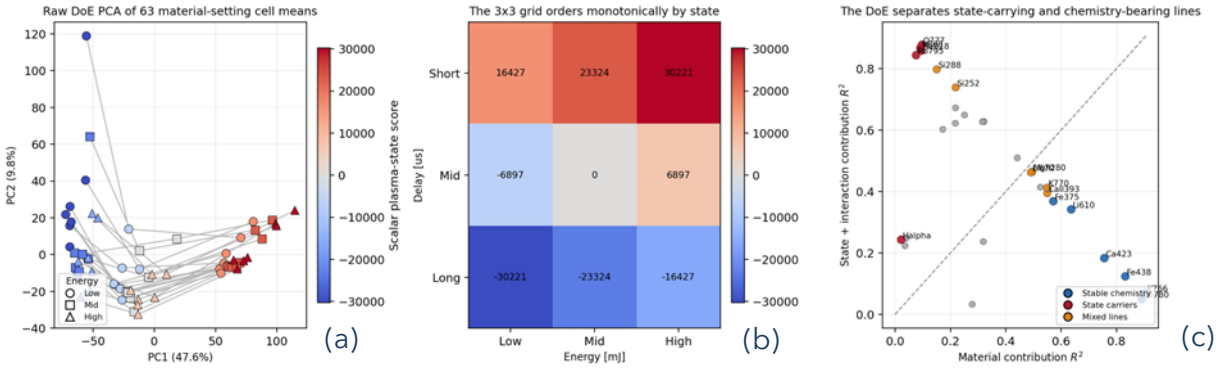

Figure 5: Controlled delay-energy variation in slurry LIBS. **(a)** DoE cell means follow a shared trajectory organized by measurement state. **(b)** The 3x3 grid orders monotonically along a scalar plasma-state coordinate dominated by delay. **(c)** Atmospheric and NIR features are strongly state-coupled; a separate set of chemistry-bearing lines remains comparatively stable.

This motivates a change in representation. Comparing absolute peak areas, a relative composition from the more stable lines, and the same composition after subtracting the shared plasma-state component, the controlled DoE becomes progressively more organized by material (Figure 6). The same direction of improvement appears in repeated-site data from independent sessions, though it is not uniform across sites. This indicates that the residual cross-session variation is not a single removable nuisance axis but is partly entangled with the provenance signal itself.

Funded by the European Union

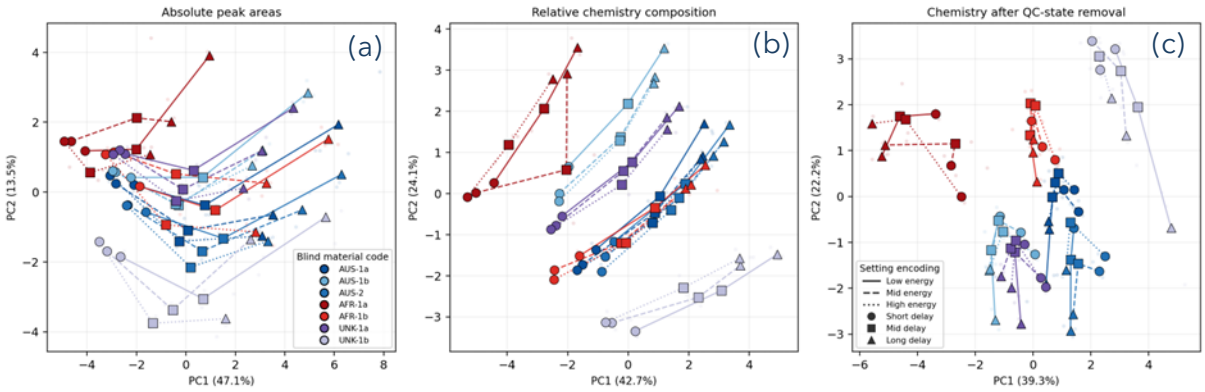

Figure 6: The controlled DoE becomes progressively more material-structured as common-mode plasma effects are suppressed. **(a)** Absolute peak areas. **(b)** Relative chemistry composition. **(c)** After QC-state removal. Faint points: individual spectra; larger markers: materials traced across the 3x3 grid.

In a site-level leave-one-measurement-session-out benchmark across five repeated origins in the feasibility study dataset, a small number of labelled reference spectra from the held-out session still improved both cross-session classification and out-of-distribution rejection (Figure 7). The benchmark comprises 13 folds, and the held-out sessions span from 9 to 103 distinct sample groups, so the comparable few-shot sweep is restricted to k <= 5. In the strongest absolute-peak baseline, three calibration spectra improved classification accuracy from 0.59 to 0.84, and unknown-origin rejection AUC from 0.89 to 0.91. The improvement was broad but heterogeneous: hard sites became partially recoverable, while already-working sites sharpened further. This points toward a calibration-based deployment model rather than a universal zero-shot approach.

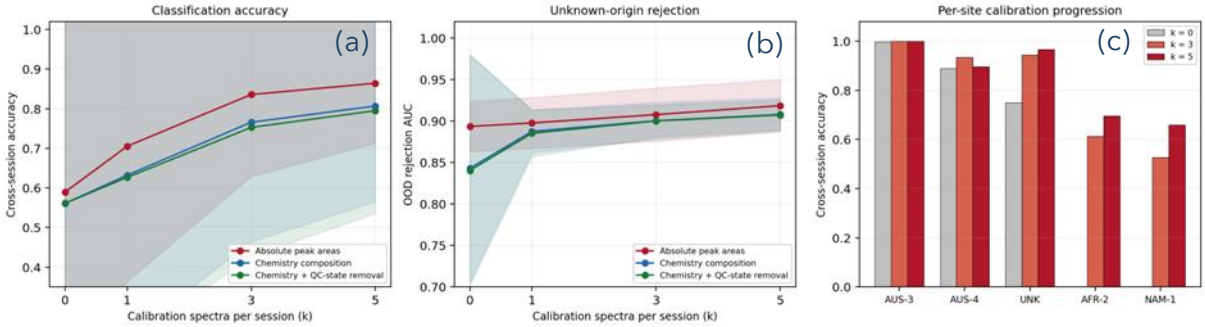

Figure 7: Few-shot calibration in a site-level leave-one-session-out benchmark. **(a)** Cross-session classification accuracy improves steeply with a small calibration budget. **(b)** Rejection of unknown-origin spectra is already plausible at zero-shot and improves further with calibration. **(c)** Per-site accuracy at k=0, 3, and 5 calibration spectra. Shaded bands in (a, b) show ±1 standard deviation across the contributing folds.

Outlook

A provenance-linked chemistry signal is present in slurry LIBS, which can be recovered when measurement conditions are controlled. The dominant instrumental variation is a shared, physically interpretable plasma-state mode that can be partially suppressed, and the residual material structure becomes more visible in compositional representations.

Universal zero-shot classification across sessions is not supported by the present dataset, but the few-shot calibration results show that a small number of reference spectra per session is sufficient to recover operationally useful classification and out-of-distribution rejection.
Future work should pursue two directions: controlled experiments varying nuisance axes beyond the current DoE (solids fraction, particle size, optics state, sample type, atmospheric conditions) to better separate provenance from session-specific variation; and tracking matched samples through the processing chain, from ore feed through concentrate to post-calcination product, to establish where the provenance fingerprint is most stable and most practically measurable.

Autoencoder-based classification

An autoencoder-based classification method was explored for the purposes of this study. An autoencoder (AE) is a neural network trained to compress its input into a low-dimensional representation and reconstruct the original from that compressed form, forcing the network to learn which spectral features carry information and which can be discarded as noise. The denoising variant used here trains on deliberately corrupted inputs (intensity perturbations, additive noise, wavelength shifts) while reconstructing the clean spectrum, encouraging the representation to capture stable spectral structure rather than measurement artifacts.

Since the AEs both compress most significant information into a low-dimensional representation and reconstruct the original form, both features could be utilized in different manners. If the AE is taught to reconstruct the original form with multiple samples of differing origins, the model will learn to find the differing aspects of each origin. Thus, the low-dimensional space could be used to group the samples and classify new unknown samples by the closest grouping and thus predict the potential origin. Another method of training would be to train multiple models of the same structure, but each model would be trained with one origin of samples, forming an ensemble of AEs. Origin classification of unknown samples would be predicted by the lowest reconstruction error.

We tested multiple normalization methods found in literature for LIBS spectra (Guezenoc, 2019). For the ensemble of AEs classification model, the best-found normalization was the standard normal variate. To mitigate learning only water and air content, H-alpha, O-I and N-I related spikes were zeroed. The classification performance can be seen in Figure 8and the f1-score was 0.78 (macro average) and 0.93 (weighted average).

Funded by
the European Union

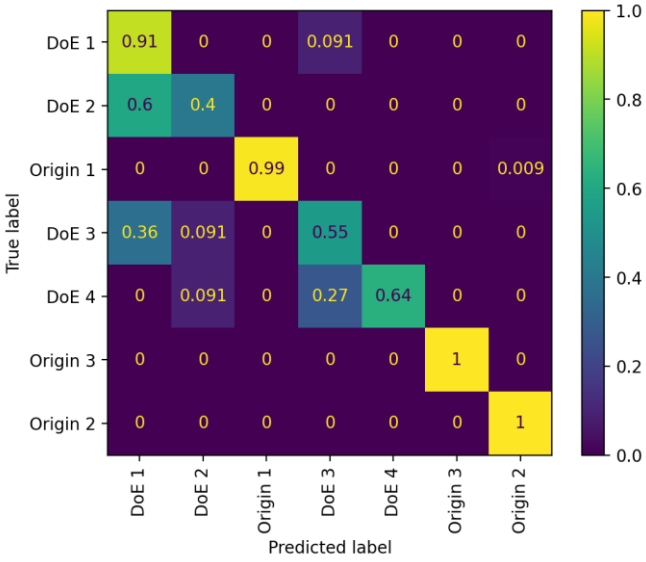

Figure 8: Confusion matrix for classification of validation dataset, not used in training. Model used: ensemble AE and classification by lowest reconstruction error. Rows are normalized. Labels 0,1,2,4 and 5 were from DoE samples, where the energy and the sample capture delay times were alternated.

As an example usage, the AEs could be trained in origin and then be used in receiving facilities to either classify samples from multiple origins and compare to sample passport information or to have the same model between the sending and receiving end to see if the reconstruction error is too high. Thus, giving a red-flag notification for further analysis.

The current study on AEs however has a few caveats due to how LIBS information is formed. Currently only the previously mentioned preprocessing and normalization methods are used. LIBS is highly susceptible to both energy and the delay between the excitation and sample capture, both of which can drift from the nominal value. In addition, the water content of the samples, temperature, optical path blockages and component failures will affect the results. Thus, further exploration into mitigating these effects needs to be done, so the autoencoders do not actually learn the water content or measurement device configurations and reduce false positives in the red-flag notifications due to just system failures, rather than sample disparities.

Funded by
the European Union

- **Method evaluation**

The Metso Courier® 8X SL online LIBS system was evaluated according to the five criteria defined in §2 Method evaluation.

Mobility (M): The Metso Courier 8X analyzer system is a containerized solution that, in principle, can be relocated between sites, for example by truck transportation. While this provides a degree of theoretical mobility, in practical operation the system is typically installed as a fixed analyzer due to the need for several permanent supply connections. Courier 8X requires pneumatics, electrical power, and water to function, which limits the ease of relocation once installed. Metso has nevertheless invested significant engineering effort into improving and safeguarding the transportability of the system, ensuring that relocation remains feasible when required. Taking into account both the containerized design and the practical installation constraints, the mobility of the Courier 8X is evaluated with a score of 2.

Production Chain Coverage (PCC): The Metso Courier 8X analyzer system is applicable at multiple stages of the lithium value chain, including ore-to-concentrate processing and concentrate feed to a lithium hydroxide (LiOH) plant. In principle, Courier 8X could be installed at the LiOH plant intake to characterize incoming concentrate. As the system is designed for slurry analysis, dry concentrate would require controlled dilution with water prior to measurement. Impurity control is critical in LiOH processing, with iron being a key detrimental impurity during the acid dissolution stage. Courier 8X may support impurity monitoring at selected upstream process points. However, uncertainty remains regarding the effect of calcination on analytical performance. The impact of calcination on LIBS spectra and on the preservation of spectral or provenance fingerprints is not verified. Based on the potential applicability from ore to concentrate and pre-LiOH plant deployment, offset by slurry preparation requirements and unresolved calcination effects, the applicability of Courier 8X in this context is assigned a score of 7, indicating partial applicability with technical and evidence-related limitations requiring further research.

Differentiating power (DP): The differentiating power (DP) of the Metso Courier 8X analyzer system was assessed against hand-held LIBS and laboratory assays. Courier 8X provides significantly higher spectral resolution and greater laser energy than hand-held LIBS, enabling separation of closely spaced elemental peaks that are blended in typical hand-held instruments. The system captures 2D CCD detector data converted into 1D spectra, offering higher information content than the regressed elemental outputs typically produced by hand-held LIBS, and supporting both qualitative and quantitative analysis. Higher detector sensitivity further enhances the detection of minor compositional differences. Classification results show that Courier 8X can discriminate between material classes. However, the provenance signal is strongly confounded by analyzer settings, atmospheric effects, and macro-scale sample properties, particularly water content, resulting in high sensitivity to measurement conditions. With improved experimental control of these confounding factors, discrimination performance is expected to improve. Based on current performance and identified limitations, the differentiating power is assigned a score of 6, indicating moderate discriminative capability with clear development potential.

Funded by the European Union

Cost of implementing (COI): The cost of implementing the Metso Courier 8X analyzer system reflects a trade-off between straightforward process integration and a high initial equipment investment. Sample preparation requirements are simple, as the system is designed for slurry analysis and supports direct online process measurements without extensive upstream handling. This limits additional auxiliary equipment, operational complexity, and ongoing manual effort. However, the overall capital expenditure for the Courier 8X analyzer system exceeds 500 k€, which represents a significant upfront investment compared to portable or simple laboratory-based alternatives. Considering the low complexity of installation and operation, but high initial equipment cost, the cost of implementing Courier 8X is assigned a score of 2. It is worth noting, though, that Courier 8X is already in use at many concentrator plants, with an existing installed base.

Operational efficiency (OE): The Metso Courier 8X analyzer system demonstrates high operational efficiency in online process applications. Typical measurement cycle time is approximately three minutes in online LIBS operation. Sample preparation complexity is low, as Courier 8X is designed to analyze slurries through automated online sampling, without extensive handling or conditioning. From a safety perspective, the system is fully enclosed during normal operation and classified as a Class 1 laser when closed, with no ionizing radiation. This provides a safer operating environment than hand-held LIBS systems, which are typically open and operator-proximate. No special operator certification or regulatory authorization is required beyond standard operational training. *The short cycle time enables large*-scale data collection and continuous time-series monitoring, supporting near-real-time tracking of process chemistry and mineralogical drift, enabling iterative model updates. Based on fast measurement throughput, low operational burden, strong safety profile, and suitability for continuous operation, the operational efficiency of Courier 8X is assigned a score of 10.

The full set of LIBS scores is given in Table 2 and shown in Figure 9.

Table 2 : GMTI score breakdown for on-line LIBS

Metric	Weight	Score	Weighted
DP	0.30	6	1.80
PCC	0.20	7	1.40
M	0.10	2	0.20
OE	0.20	10	2.00
COI	0.20	2	0.40
TOTAL (GMTI)			**5.80**

Funded by the European Union

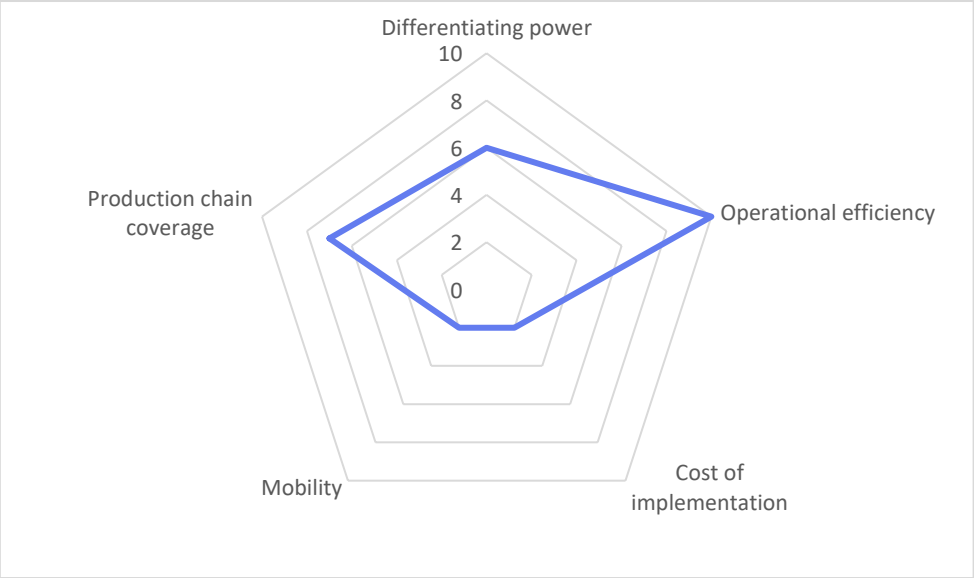

Figure 9: Method evaluation diagram for on-line LIBS.

Funded by the European Union

3.2.1.2 Mobile µLIBS

- **Instruments description and samples preparation**

The Ablascan™ system developed by Ablatom is a high-throughput chemical imaging platform based on Laser-Induced Breakdown Spectroscopy (LIBS), specifically designed for rapid, large-area elemental mapping (Figure 11). It typically achieves a spatial resolution on the order of tens of µm (approximately 10–50 µm depending on the configuration) through high repetition-rate laser ablation. The system integrates multiple spectrometers (generally between two and four), enabling coverage of a wide spectral range from the ultraviolet to the near-infrared (UV–VIS–NIR). This configuration allows for the simultaneous detection of both light elements (such as Li and H) and heavier elements. Analyses are commonly performed under a controlled argon atmosphere, which enhances plasma stability, improves the signal-to-noise ratio, and lowers detection limits, particularly for light elements. In addition, advanced data processing workflows allow for quantitative or semi-quantitative elemental mapping with minimal sample preparation.

Within the framework of the MADITRACE project, we deployed the Ablascan system in the BRGM pilot hall to test the instrument under industrial conditions. For this test, the machine was transported from Lyon to Orléans (France), and only one hour was required between its arrival and the first analyses (Figure 10). The instrument used was equipped with 3 spectrometers, covering a spectral range from 240 to 950 nm. Analyses were conducted at a spatial resolution of 20 µm on pressed pellets with a diameter of 1/2 inch (Figure 12). Each pellet consisted of 1 g of sample mixed with 0.05 g of wax acting as a binder. The ablated surface corresponded to an area of 8.52 × 8.52 mm, with a total acquisition time of 9 minutes and 30 seconds per sample.

A total of 34 elements, ranging from major to trace levels, were initially mapped. However, several elements were excluded from further analysis: carbon (C), oxygen (O), and hydrogen (H) due to contamination from the binder; sulfur (S) due to inconsistencies linked to detector changes between analytical sessions; and hafnium (Hf), which was not detected. The final dataset therefore includes 29 elements: Al, B, Ba, Be, Bi, Ca, Cr, Cs, Cu, F, Fe, K, Li, Mg, Mn, Mo, Na, Nb, P, Pb, Rb, Si, Sn, Sr, Ta, Ti, Y, Zn, and Zr. Each elemental map consists of 181,476 pixels, corresponding to high-resolution images of 426 × 426 pixels per element. The resulting dataset can be described as a set of hyperspectral maps, where each pixel contains multi-element information for the 29 retained elements.

Figure 10: Pictures of the Ablascan installation in the BRGM pilot hall.

Figure 11: Picture of the Ablascan device manufactured by Ablatom used as part of the MADITRACE project, and the machine's main features.

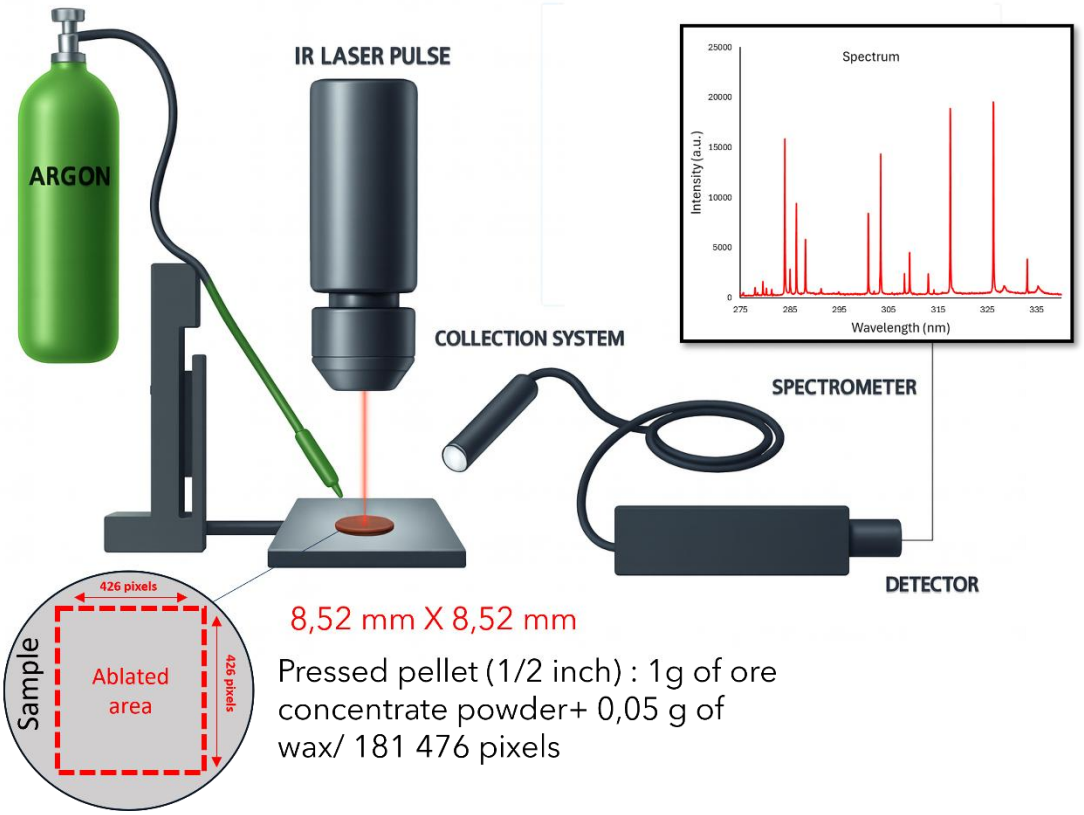

Figure 12: The principle of the Ablascan device used in the MADITRACE project.

Funded by the European Union

- **Samples**

The sample corpus comprises 30 samples, including both concentrates and raw ores, originating from a range of deposits worldwide. All samples are in powder form as a result of extraction processes (e.g., flotation). Samples sharing the same identification number were supplied by the same provider. The dataset is predominantly composed of spodumene concentrates, with the exception of the French samples, which consist of lepidolite-bearing materials. Additionally, one sample of zinnwaldite concentrate from a Central European deposit is included.

Table 3 : summary of analysed sample information. Samples were labelled as "training "when the total of samples is enough to train the model per mine or as 'unseen' when the total number of samples is below 4. Samples where replicates analyses were performed are annotated by black-filled cell in r.

id.	number of samples	Category	Mine	r.	Training or unseen
Li37	1	Spodumene concentrate	Australia-1		Training sample
Li38	1	Spodumene concentrate	Australia-1		Training sample
Li45a-j	10	Spodumene concentrate	Australia-1		Training samples
Li43a-e	5	Spodumene concentrate	Australia-2		Training samples
Li35	1	Spodumene concentrate	Canada-1		Training sample
Li36	1	Spodumene concentrate	Canada-1		Training sample
Li46a-u	20	Spodumene concentrate	Canada-1		Training samples
Li20	2	Spodumene concentrate	Finland		Training samples
Li57	1	Spodumene concentrate	Finland		Training sample
Li60	1	Spodumene concentrate	Finland		Training sample
Li31	1	Lepidolite concentrate	France		Training sample
Li32	1	Lepidolite concentrate	France		Training sample
Li48	1	Lepidolite mineral	France		Training sample
Li55a-j	10	Lepidolite mineral	France		Training samples
Li56	1	Lepidolite concentrate	France		Training sample
Li62	1	Lepidolite concentrate	France		Training sample
Li81a-o	14	Lepidolite concentrate	France		Training samples
Li58	1	Spodumene mineral	Portugal-1		Training sample
Li66	1	Spodumene mineral	Portugal-1		Training sample
Li67	1	Spodumene concentrate	Portugal-1		Training sample
Li70a-g	7	Spodumene mineral	Portugal-1		Training samples
Li69	1	Spodumene concentrate	Australia-3		Unseen sample
Li33	1	Spodumene concentrate	Austria		Unseen sample
Li34	1	Spodumene concentrate	Canada-2		Unseen sample
Li28	1	Spodumene concentrate	Canada-3		Unseen sample
Li21	1	Spodumene concentrate	Canada-4		Unseen sample
Li50	1	Zinnwaldite concentrate	Middle Europe		Unseen sample
Li49	1	Lepidolite mineral	Portugal-2		Unseen sample
Li59	1	Petalite mineral	Portugal-3		Unseen sample
Li61	1	Spodumene concentrate	Sweden		Unseen sample

Funded by the European Union

- **Method description**

We developed a machine learning framework to discriminate Li deposits based on high-resolution chemical maps acquired by LIBS. The approach is specifically designed to powder samples, for which spatial information is inherently non-reproducible, by focusing instead on elemental co-occurrence patterns at the pixel scale.

(1) **Sample preparation & LIBS data acquisition**

The sample preparation and their analysis by µLIBS are described in the paragraph above.

(2) **Elemental combination strategy**

Unlike conventional imaging approaches, this study does not directly exploit spatial structures. Instead, it assumes that elemental co-occurrence at the pixel level reflects the mineralogical composition of powders, even when grain positions are random. A binary thresholding approach is applied: for each pixel, elements with intensity values above zero are considered present. These elements are then combined to form elemental combinations (co-occurrence patterns) (Figure 13). Each sample is thus described by a feature vector where: (1) columns correspond to unique elemental combinations, (2) values correspond to the number of pixels exhibiting each combination. To reduce noise and dimensionality, combinations covering very few pixels are filtered out using a pixel-count threshold optimization. The optimal threshold (~2000 pixels, ~1.1% of the map) is selected based on a trade-off between: classification accuracy, number of retained features and statistical robustness.

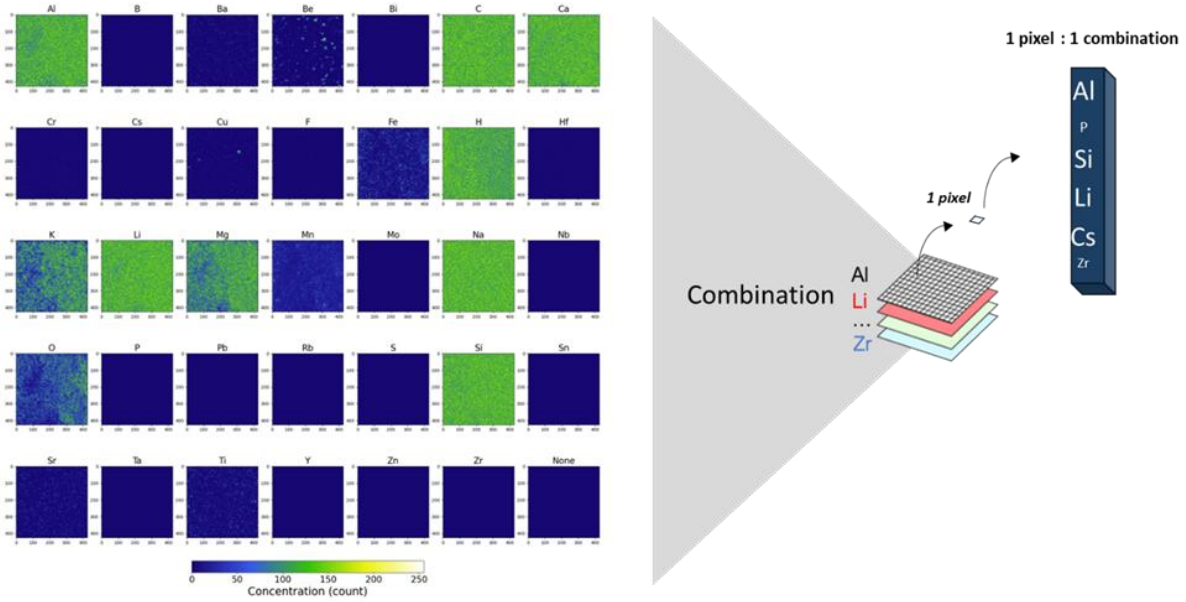

Figure 13: example of visualisation of chemical maps per investigated element for a spodumene concentrate.

(3) **Machine learning framework**

The classification task is performed using a Random Forest (RF) algorithm, chosen for its robustness to noise, ability to handle high-dimensional data, and reduced overfitting compared to single decision trees. A one-vs-rest (OvR) strategy is implemented: one RF model is trained per deposit, each model learns to distinguish a given deposit from all

Funded by the European Union

others (Figure 14). This approach allows: 1) independent classification of each deposit, 2) easy integration of new deposits without retraining the entire system. Model performance is evaluated using Leave-One-Out Cross-Validation (LOO-CV), where each sample is iteratively excluded from training and used for testing. This is particularly suited to small datasets and provides an unbiased estimate of predictive performance.

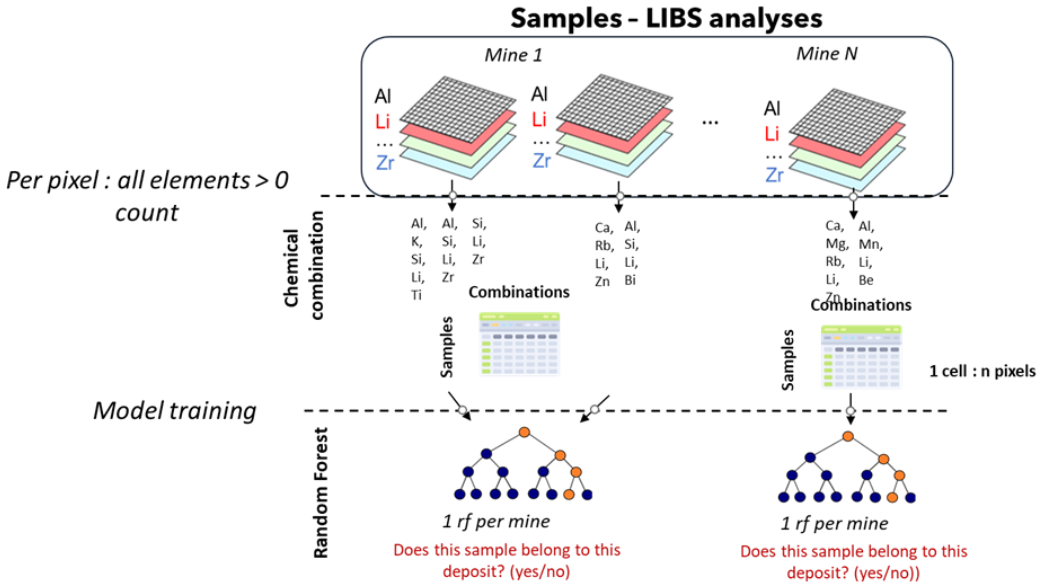

Figure 14: strategy developed to LIBS maps processing and classification.

(4) **Model Interpretation and feature Analysis**

To interpret the model and identify the most discriminant features, the study combines Random Forest feature importance with SHAP (SHapley Additive exPlanations) values. SHAP provides a local interpretation of each prediction by quantifying the contribution of each elemental combination to the classification outcome. This allows identification of: (1) key combinations associated with lithium minerals (spodumene, lepidolite), (2) combinations linked to impurity phases or accessory minerals, which play a major role in deposit discrimination. The most influential combinations are further analyzed using Principal Component Analysis (PCA), demonstrating that they are sufficient to reproduce the clustering of deposits in an unsupervised space (Figure 15).

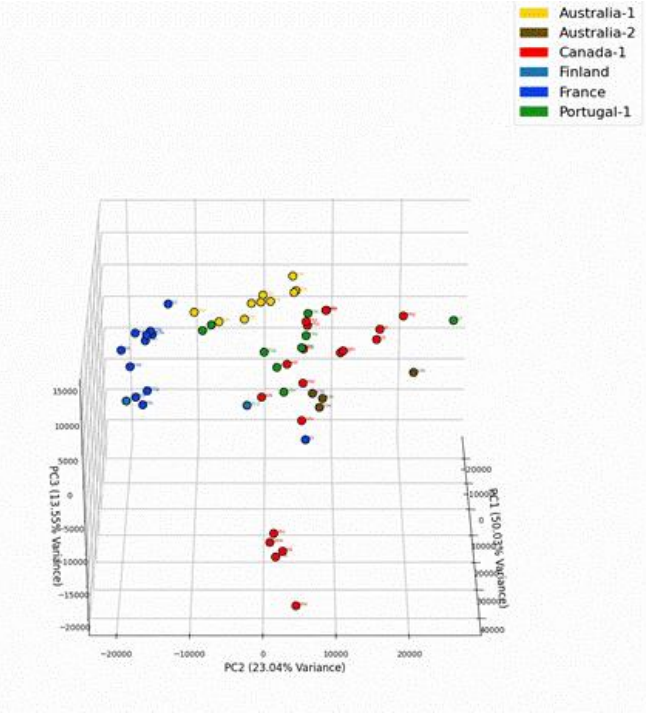

Figure 15: Example of ACP visualization.

- **Results**

(1) Elemental maps and combination structure

The LIBS imaging performed using the Ablascan system produced high-resolution elemental maps for each sample, with each map consisting of 426 × 426 pixels per element. Figure 16 illustrates a representative elemental distribution for a spodumene sample (Li46n – Canada-1). The maps reveal contrasted spatial distributions depending on the element. Major elements such as Al or Si exhibit relatively homogeneous distributions across the sample, whereas trace elements such as Cs or Rb are localized in sparse and discrete zones. This heterogeneity supports the hypothesis that elemental co-occurrence patterns reflect mineralogical associations, even in powdered samples where spatial continuity is lost. The extraction of elemental combinations at the pixel scale resulted in a very large feature space, reaching up to approximately 20,000 combinations when no filtering is applied. This highlights both the richness of the chemical information contained in LIBS maps and the need for an appropriate dimensionality reduction strategy.

Funded by the European Union

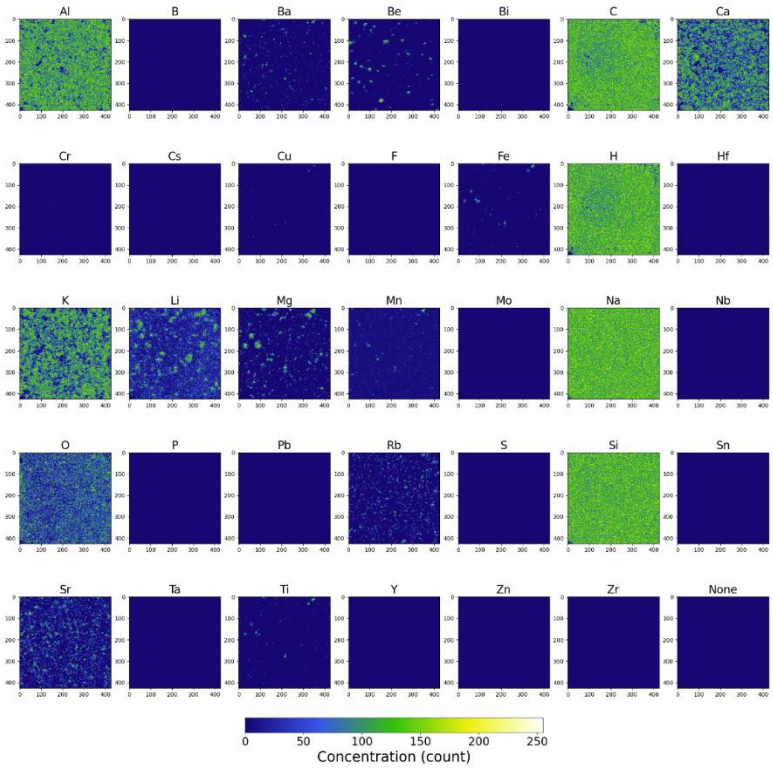

Figure 16: example of elemental concentration map from ABLASCAN for one spodumene mineral sample (Li46n – Canada-1).

(2) Pixel threshold selection and dimensionality reduction

To reduce dimensionality and improve statistical robustness, a filtering strategy based on the minimum number of pixels per elemental combination was implemented. Figure 17a shows the evolution of both the number of combinations and the classification accuracy (LOO-CV) as a function of the pixel threshold. At low thresholds, the number of combinations remains very high, which increases the risk of overfitting and limits interpretability. Increasing the threshold leads to a rapid decrease in the number of retained combinations, while classification accuracy remains stable around 0.87. Beyond a certain point, however, the accuracy begins to decrease, indicating that overly restrictive filtering removes relevant discriminant information. The optimal threshold was determined by balancing classification performance, feature reduction, and statistical robustness (Figure 17b). The selected threshold corresponds to approximately 2000 pixels, representing about 1.1% of the total map area. This result indicates that the most informative chemical signatures are associated with combinations that cover a sufficient number of pixels to be statistically meaningful.

Funded by
the European Union

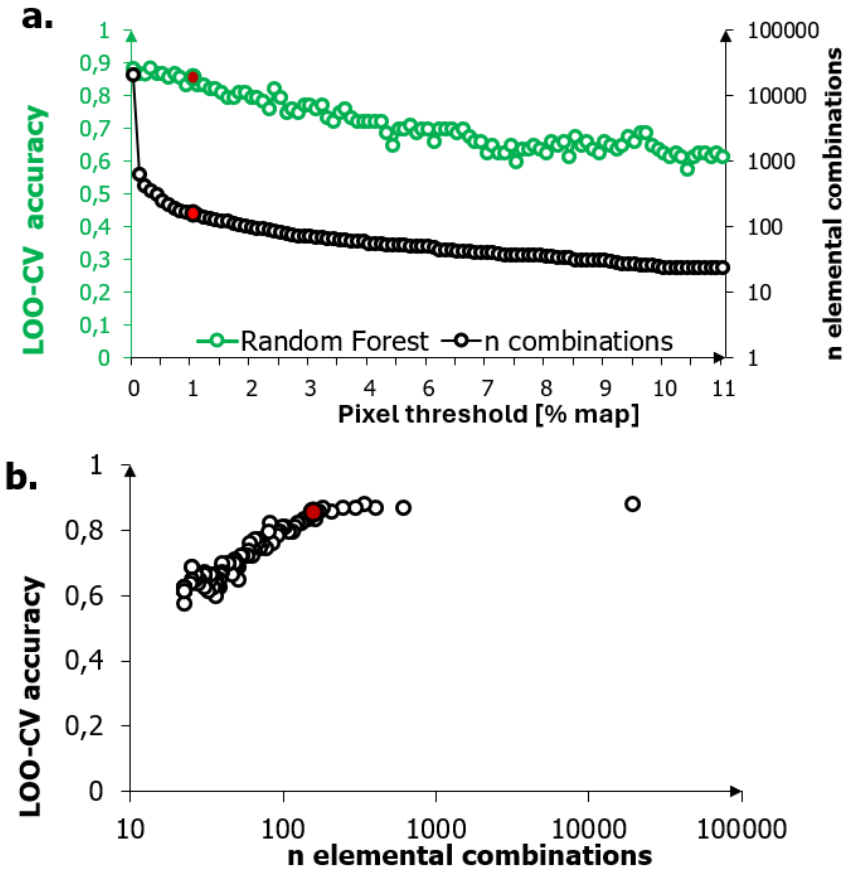

Figure 17: a. model accuracies by LOO-CV and number of combinations considered according to the pixel count threshold. b. accuracies and number of combinations relationship. The red dot represents the best configuration estimated by calculating the Euclidean distance between these features.

(3) Classification performance

Overall model accuracy. The classification performance was evaluated using Leave-One-Out Cross-Validation (LOO-CV). The confusion matrix presented in Figure 18 shows a high level of accuracy across the six training deposits, with an overall accuracy of approximately 88.9%. Most samples are correctly classified, with only a limited number of misclassifications observed. Notably, the Canada-1 deposit achieves perfect classification. These results demonstrate that elemental co-occurrence patterns extracted from LIBS maps provide sufficient information to discriminate between lithium deposits, despite the absence of meaningful spatial organization in powder samples.

Funded by the European Union

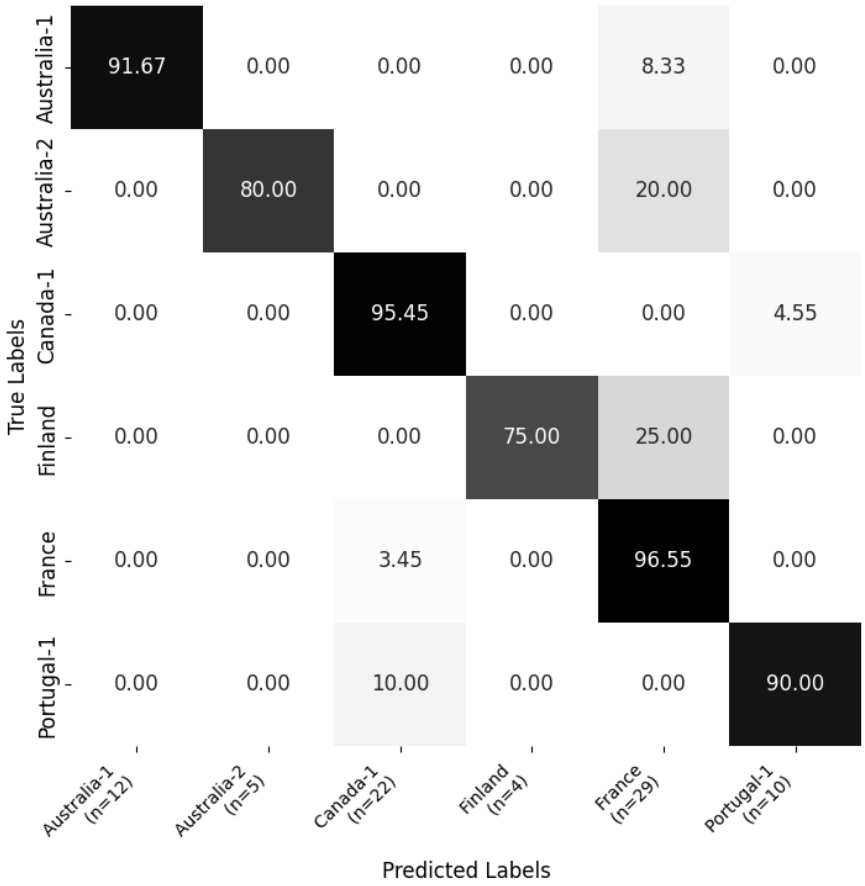

Figure 18: deposit classification accuracy estimated from LOO-CV. X axis displays the predicted labels with the number of samples per each class, while Y axis displays the true labels -*easter egg*. The diagonal here highlights a good classification for all 6 deposits.

Prediction probabilities and model confidence. Prediction probabilities for each sample are shown in Figure 19. Most deposits exhibit high probabilities of correct classification, particularly Australia-1, Canada, and France, where average probabilities are around 80%. Moderate probabilities are observed for Portugal and Australia-2, while Finland shows lower confidence, likely due to the limited number of training samples. Some samples display intermediate probabilities across multiple deposits, reflecting overlapping chemical signatures between geological environments. This behaviour is consistent with the natural variability of mineral assemblages and does not necessarily indicate model failure.

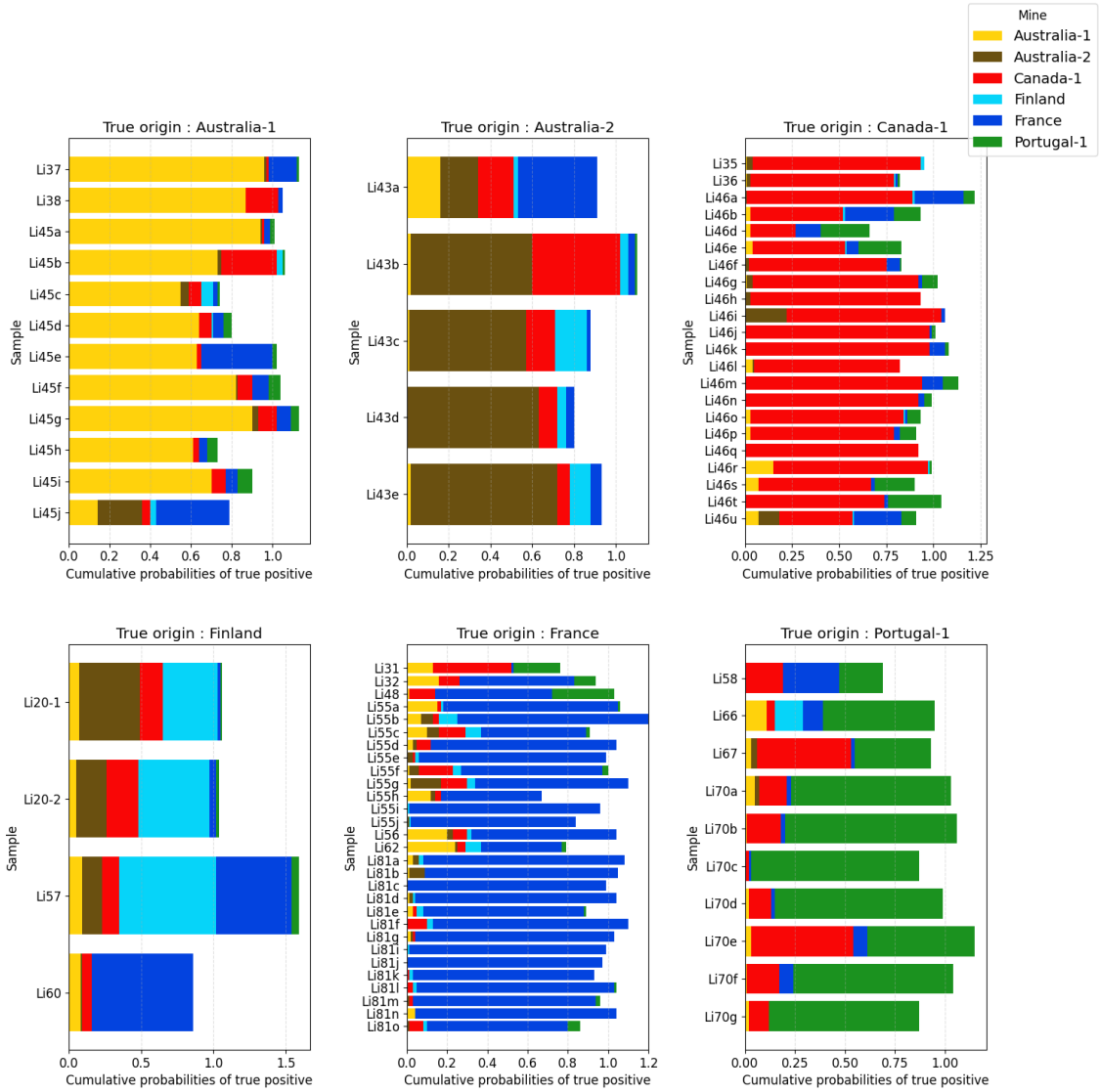

Figure 19: predicted deposit probabilities per sample. Each subplot is related to the deposit. Finland group excepted, each model overall shows high probabilities to belong to their deposit.

Generalization to unseen samples. Predictions performed on unseen deposits (Figure 20) show moderate to high probabilities of assignment to known classes. Although these samples were not included in the training dataset, the model is able to identify similarities with existing deposits, suggesting that the extracted features capture generalizable geochemical signatures.

Funded by the European Union

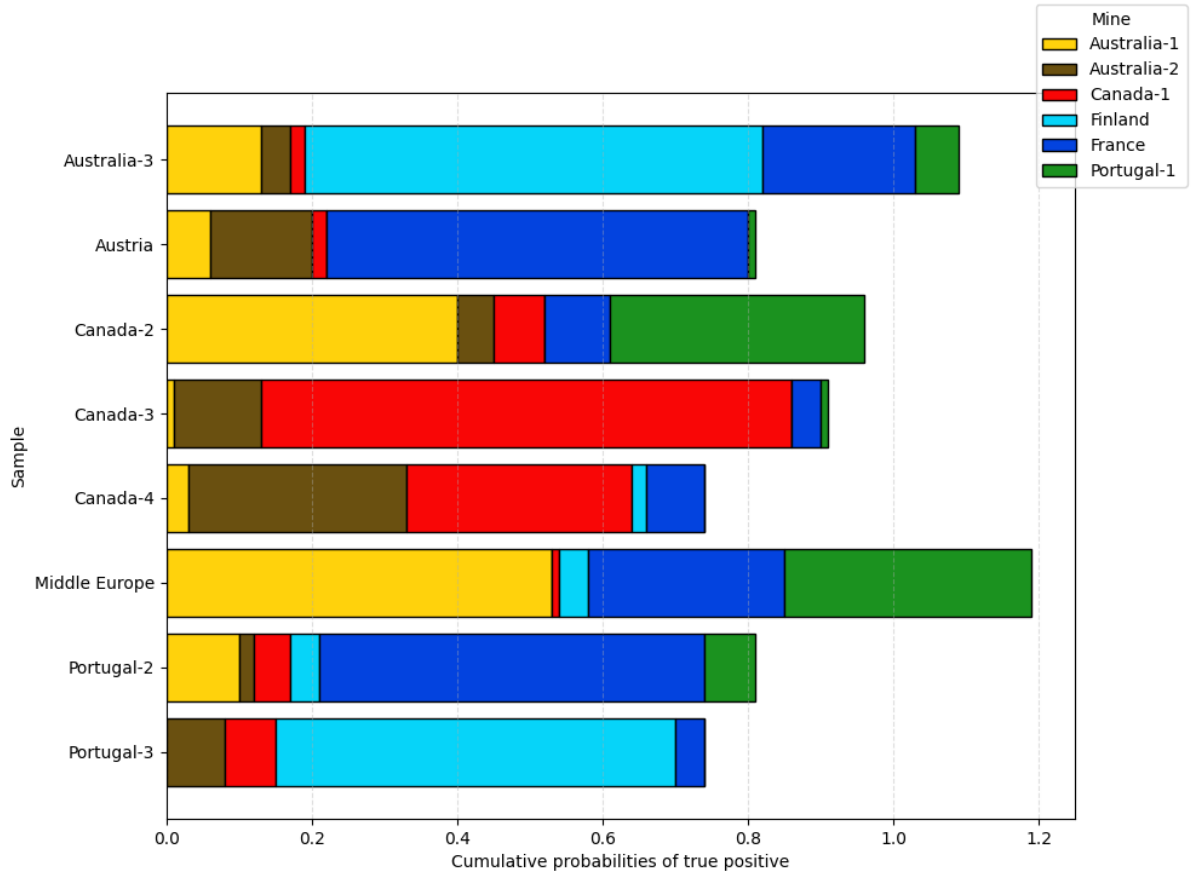

Figure 20: Predictions of probabilities for the unseen deposits.

(4) Feature importance and interpretation

Random forest feature importance. Feature importance analysis indicates that each deposit is characterized by a relatively large number of elemental combinations, typically around 90. The most important features contribute between 8% and 14% to the classification. However, the large number of contributing features complicates interpretation and may introduce biases related to the random forest training process.

SHAP analysis: identifying discriminant combinations. To improve interpretability, SHAP values were computed to quantify the contribution of each combination to the model predictions. Figure 21 presents beeswarm plots of the most discriminant combinations for each deposit. These results highlight the importance of both lithium-bearing mineral signatures and impurity-related elements. An apparent inversion pattern is observed, where high feature values are sometimes associated with negative SHAP values. This behaviour arises from the one-vs-rest classification framework, in which combinations that are abundant in other deposits may act as negative indicators for the target class. Despite this effect, the selected combinations remain strongly discriminant, as confirmed by their ability to separate deposits in subsequent analyses.

Funded by
the European Union

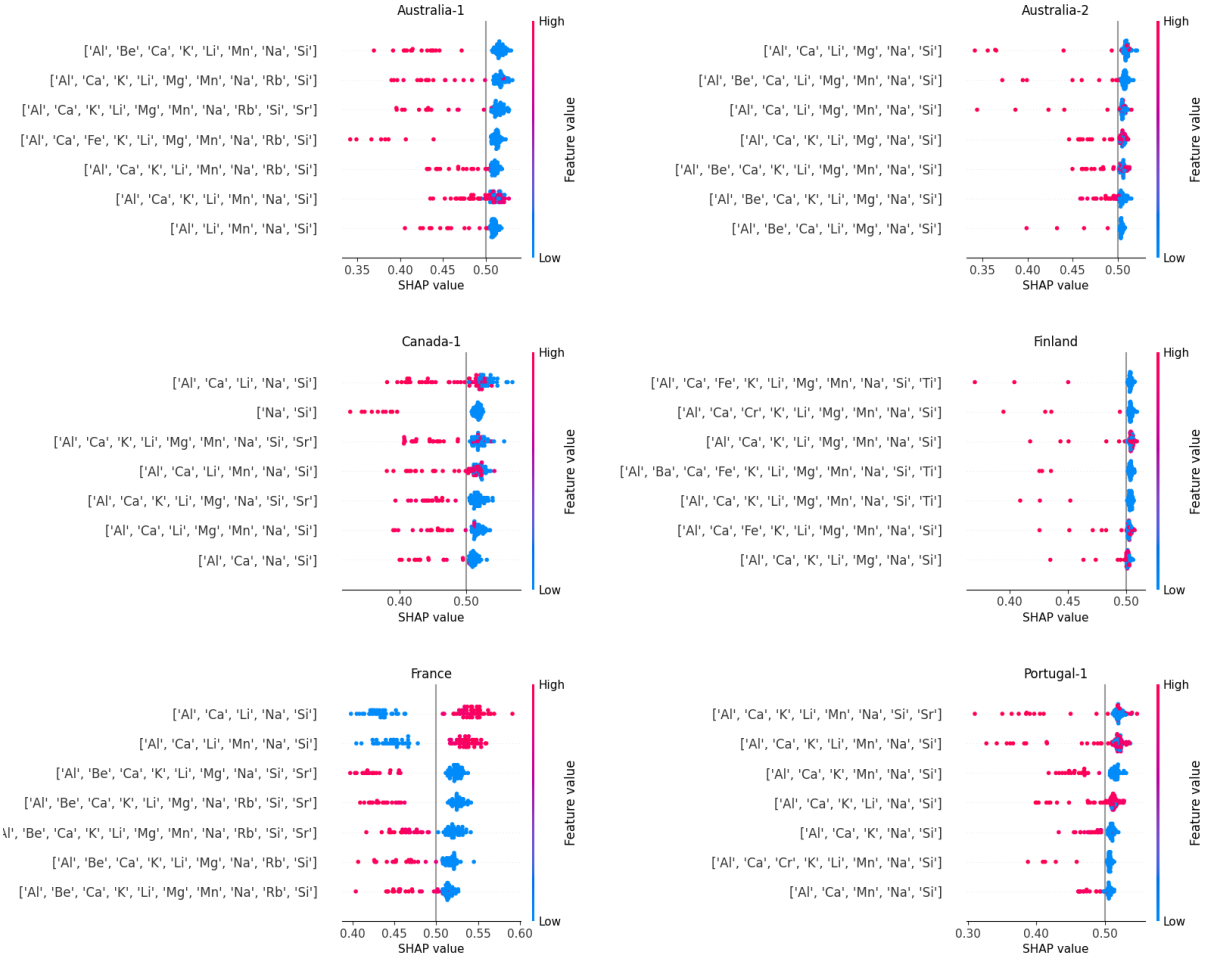

Figure 21: Beeswarm plots per deposit of elemental combination importance ranking according to SHAP values. The seven most discriminating features were plotted here. The colour gradient displays the log of the number of pixels per combination. If the SHAP value is lower than the baseline for high pixel numbers (i.e. red dots) and higher SHAP value for less pixel numbers (i.e., blue dots), then the combination discriminates the other deposits.

Multivariate validation of discriminant features. A PCA was performed using the most influential combinations identified by the SHAP analysis. The resulting biplots (Figure 22) show clear clustering of samples according to their deposit of origin, with a total explained variance of approximately 70.6%. Some misclassified samples are located close to other deposit clusters, indicating shared chemical characteristics. In addition, certain deposits, such as Canada-1, display internal variability, which may reflect geological heterogeneity or differences in processing history.

Funded by the European Union

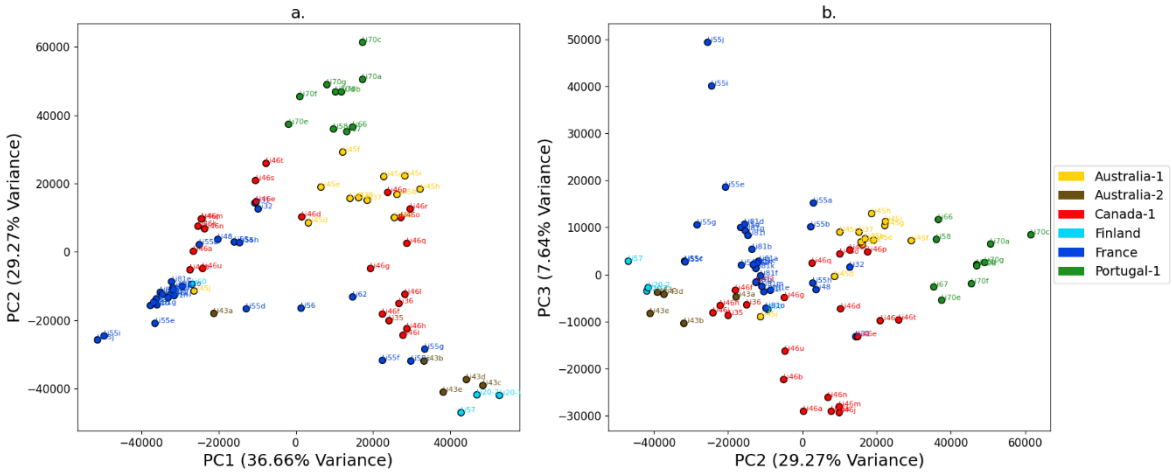

Figure 22: PCA biplots of the training dataset using a. first and second components and b. second and third components with a total explained variance of 70.6 %. The PCA was conducted on the number of pixels covered per the combinations selected by the SHAP algorithm. Deposit are highlighted by colors and sample id. are displayed as well.

- **Discussion and implications**

The results demonstrate that elemental co-occurrence patterns extracted from LIBS imaging provide a robust and interpretable basis for lithium deposit discrimination. By focusing on pixel-level combinations rather than spatial structures, the method overcomes the limitations associated with powder samples while preserving meaningful mineralogical information. A key finding of this study is the importance of impurity-related elements in discriminating deposits. These elements, which are often inherited from the geological environment or only partially removed during processing, constitute reliable fingerprints of origin. This highlights the potential of LIBS-based chemical imaging for traceability applications along the critical raw materials supply chain. Some limitations remain, including the relatively small number of samples for certain deposits and the potential impact of preprocessing choices. Future work should focus on expanding the dataset, integrating additional stages of the supply chain, and assessing the transferability of the approach across different instruments.

- **Method evaluation**

The mobile µLIBS (Ablascan™) technique was evaluated according to the five criteria defined in §2 Method evaluation (Figure 23, Table 4).

Mobility (M): The mobile µLIBS system (Ablascan™) can be considered transportable rather than fully mobile. While the instrument is not permanently fixed and can be moved between locations, it requires a controlled operating environment, including the use of an argon atmosphere, and relies on laboratory-type sample preparation (pressed pellets). Its size and infrastructure requirements limit its deployment directly in field conditions. According to the defined mobility scale, this corresponds to a semi-mobile solution requiring dedicated setup, resulting in an estimated score of 4/10.

Production Chain Coverage (PCC): Mobile µLIBS demonstrates applicability across several stages of the upstream lithium production chain, particularly for ores and concentrates in powder form. The method is well suited for processed mineral samples obtained after comminution and flotation. However, its applicability to downstream stages (e.g., refined chemicals or final products) is not demonstrated, and the requirement for sample preparation limits its use in continuous or in-line processes. Therefore, the technique covers a significant but incomplete portion of the value chain, corresponding to a score of 4/10.

Differentiating Power (DP): The differentiating power of mobile µLIBS is very high, as demonstrated by the strong classification performance obtained using machine learning approaches. The method leverages high-resolution elemental maps and pixel-level elemental co-occurrence patterns, enabling robust discrimination between lithium deposits. Reported results show an overall classification accuracy close to 89%, supported by advanced data analysis techniques such as Random Forest, SHAP interpretation, and PCA validation. These results indicate excellent discrimination capability with high assignment accuracy, justifying a score of 8/10.

Cost of Implementation (COI): The cost of implementing the mobile µLIBS system is relatively high, with an estimated instrument cost of approximately €300,000. In addition to the capital investment, operational costs include sample preparation (pelletizing with binder) and consumables such as argon gas. Although the method does not require extremely complex preparation, these additional requirements increase the overall cost of use. According to the cost scale defined in the methodology, this places the technique in the category of high-cost systems with preparation needs, resulting in a score of 6/10.

Operational Efficiency (OE): The operational efficiency of mobile µLIBS is moderate. Each analysis requires approximately 9 minutes and 30 seconds per sample, which is relatively long compared to rapid screening techniques. Furthermore, sample preparation steps (pellet pressing) introduce additional time and operational constraints. The need for controlled atmosphere conditions and laboratory-type handling further reduces throughput and flexibility. While the method provides high-quality data, these constraints limit its efficiency in large-scale or real-time applications, corresponding to a score of 6/10.

Overall, with a GMTI score of 6/10 (Table 4), the mobile µLIBS technique can be considered a balanced solution with strong differentiating power but moderate coverage and operational constraints, making it well suited for targeted traceability applications rather than full-chain, real-time deployment.

Funded by the European Union

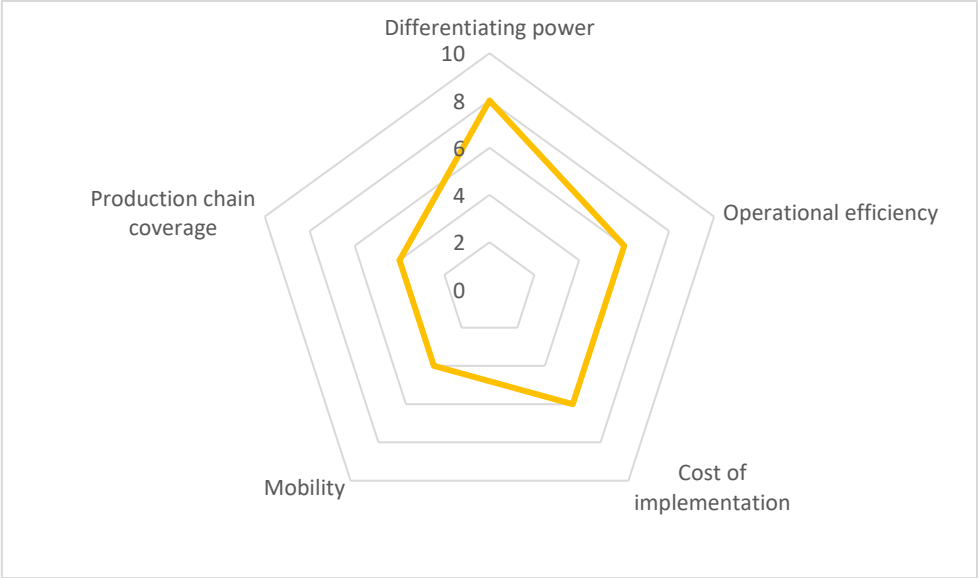

Figure 23: Method evaluation diagram for mobile µLIBS.

Table 4 : GMTI score breakdown for mobile µLIBS.

Metric	Weight	Score	Weighted
DP	0.30	8	2.4
PCC	0.20	4	0.8
M	0.10	4	0.4
OE	0.20	6	1.2
COI	0.20	6	1.2
TOTAL (GMTI)			**6**

Funded by the European Union

3.2.2 Methods based on mineral luminescence: UV Bench & cathodoluminescence microscope

3.2.2.1 Mineral luminescence principle

Luminescence regroups all the phenomena of light emission by a substance that is not incandescence (i.e. the emission of light caused by high temperature often referred to as black body radiation). The luminescence occurs as a response to the excitation of the matter by an external stimulus. In the case of geosciences, mainly two types of luminescence are used for rock characterisation: fluorescence and cathodoluminescence. The source of the luminescence in the case of fluorescence is a photon (i.e. a source of light). Some minerals show a good response to UV-light in particular. In the case of cathodoluminescence, the stimulus for luminescence is an electron beam.

Fluorescence and cathodoluminescence rely on similar physical principles. In quantum physics, atoms are represented with quantified energy levels that are filled with electrons. These levels are called electron orbitals and can accept a limited number of electrons. They are filled in starting from the orbitals with the lowest energy and until all electrons associated with the atomic nucleus have a position in this energetic structure. The last fully filled orbital is called the valence orbital and the first incompletely filled orbital is called the conduction orbital (Figure 24). These two orbitals contain the electrons implicated in the chemical reactivity of the atom, thus mobile electrons sensitive to external stimuli.

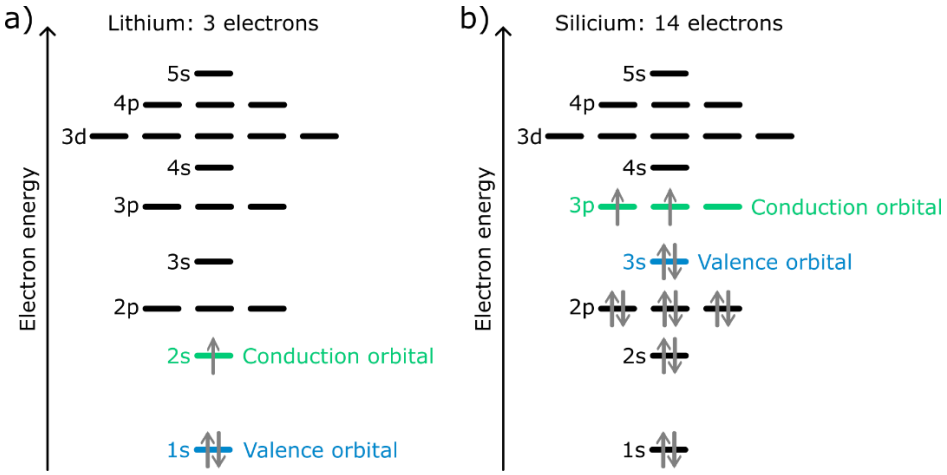

Figure 24: Schematic representation of electronic orbitals for lithium (a) and silicium (b). Electrons are represented by arrows. Orbitals are represented by one or several lines horizontally aligned with their names indicated on their left side. An orbital is full when all the lines have two electrons on them.

A material or mineral being the combination of many atoms, its quantum structure is more complex with bands of energy instead of the well-defined energies of the atomic orbitals. The overall structure stays similar and both a conduction band and a valence band can be defined. However, the complex atomic combination is responsible for the occurrence of metastable energy levels, often referred to as electron traps, that are responsible for luminescence. When excited by an external stimulus (UV-light or electrons in our case), energy is transferred to electrons in the material structure. This energy addition triggers movement of excited electrons between the valence and conduction bands and the electron traps located in-between potentially leading to the emission of light as electrons get de-excited (Figure 25).

Funded by the European Union

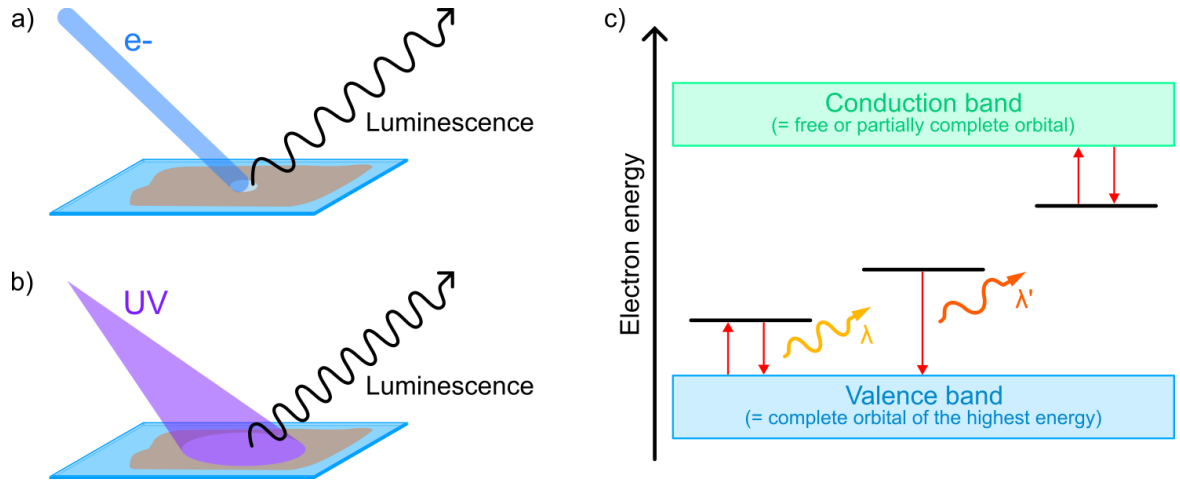

Figure 25: Principle of luminescence. a) Schematic representation of cathodoluminescence: the surface of the sample (here a rock thin section) is swept using an electron beam which can produce a luminescence. b) Schematic representation of UV-luminescence: the surface of the sample is swept using a UV light which can produce a luminescence. c) Schematic representation of electron traps responsible for luminescence. Red arrows indicate electron energy evolution.

The occurrence and energies of the electron traps, thus the luminescence, is controlled by material atoms arrangements and chemical composition. Even very low quantities of some elements can have a strong influence on the luminescence (e.g. Kempe & Götze, 2002). Luminescence techniques consequently have an excellent potential for material fingerprinting.

Cathodoluminescence in geosciences is in general rather used for characterization, to highlight structures that would be invisible to other analytical methods, but lately a few studies have shown its interest in source tracing (e.g. Augustsson & Reker, 2012; Baele et al., 2019).

In the case of UV light, this technique is particularly used in petroleum studies as organic matter is particularly sensitive to it (e.g. Liu et al., 2014). Apart from this, its current use in geosciences is limited. However, the fundamental similarity and complementarity with cathodoluminescence (different stimuli can trigger different electron traps) make it worth exploring for traceability applications.

3.2.2.2 Instruments description and sample preparation

UV-bench

The UV-bench used for this method development is a custom prototype made by TerraAnalytix (the company went bankrupt since). It allows the analysis of powdered samples, sand, pellets, or small rocks. It consists of a black box designed to take pictures of the sample under white light, short wavelength UV (254 nm), and long wavelength UV (between 350-365 nm).

Figure 26: UV bench prototype developed by BRGM/TerraAnalytix. Samples are introduced inside the UV bench using a plastic drawer (right picture).

MaDiTraCe samples tested with this technique are powders from ores and Li-mineral concentrates. Samples are introduced one by one in the system through a drawer at the back of the device. The powder is poured in a plastic sample holder insensitive to UV light and its surface is flattened using a glass plate. The picture acquisition is started using the included software. Three pictures under the three light sources are automatically taken (Figure 27). The sample holder is cleaned with ethanol between every sample. Analyzing one sample takes a few minutes including cleaning.

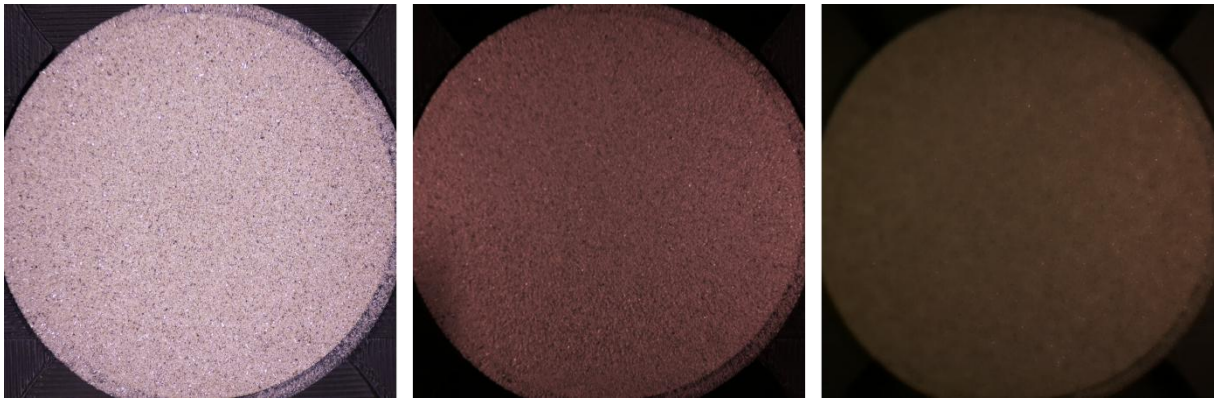

Figure 27: Example of UV bench analytical result for sample Li20. From left to right: white light picture, short UV (254 nm) picture, and long UV picture (350-365 nm). Images are 5 cm large.

One limitation of the system is the impossibility to focus on the sample and the absence of a zoom functionality. The focal point is at a fixed distance, corresponding to the top of the sample holder. This limitation is also what makes this system very simple to use.

Optical cathodoluminescence system

The Newtec Cathodyne system at BRGM (Figure 28) is a cold cathodoluminescence automated system installed on an optical microscope. The sample chamber is under vacuum during the analysis and is fitted for small samples with a flat surface, from thin

Funded by the European Union

sections to pucks and pellets. It is possible to use double-sided tape on a glass plate to analyze small particles but the vacuum state inside the sample chamber, necessary for the electron beam stability, prevents the direct analysis of powdered samples. This system is completely automated meaning that the electron beam intensity and voltage is automatically regulated according to the user's requirements, and that the stage is automated, which allows for the easy and quick creation of large mosaic images of the samples (Figure 29). Focus stays manual though.

Samples from MaDiTraCe that have been tested under cathodoluminescence are mostly powdered ores and Li-mineral concentrates. To be analysed, these had to be pressed into 13 mm diameter pellets (ca. 1 g). 5 wt% of wax binder has been added to each sample to improve the solidity of the pellets and make their manipulation easier. The wax binder has been previously tested under cathodoluminescence to ensure its own luminescence won't affect the luminescence of the samples.

A custom 3D-printed sample holder has been created. It has several advantages: 1) it allows to introduce 8 pellets at the same time in the machine, which helps to shorten analytic time (vacuum and electron beam stabilisation times are reduced), and 2) It provides fixed positions for the pellets, making the mosaics positions easier to program. However, the plastic used for 3D-printing burns under the electron beam, contributing to dirtying the electron canon, thus a metallic sample holder would be an improvement of the current design.

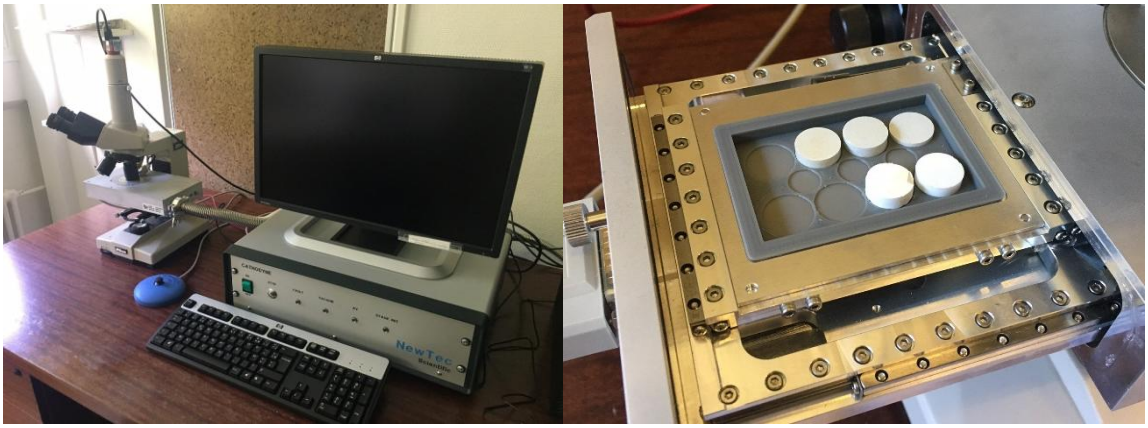

Figure 28: On the left, the Cathodyne cold cathodoluminescence system from NewTec in BRGM laboratories. The system is installed on an optical microscope and linked to a computer and a vacuum pump not visible on the picture. On the right, the custom 3D-printed sample holder in the drawer of the sample chamber.

There are different types of parameters that can be adjusted for cathodoluminescence analysis. The first type is camera parameters. The raw analytical result provided by this technique is an image that is taken from a camera. It is possible to play on the camera sensitivity to red, blue and green, which can greatly affect the colour of the images. For these tests, we fixed the white balance to the factory setting by reinitializing it at the beginning of each analytical session. Another accessible parameter in the gain, fixed to 1000 during acquisition. Finally, the exposition time can be adjusted. For the MaDiTraCe samples, we made this parameter vary between 50 ms and 5 s to adapt to samples luminescence intensity. The second type of adjustable parameters is linked to the electron beam. Two parameters can be adjusted: the tension of the electron beam, corresponding to the quantity of electron sent to the sample and the voltage, corresponding to the energy

of the electron sent to the sample. Changing the tension will mostly impact the intensity of the luminescence. This value has been fixed to 200 µA as imaging one sample at different tensions has little interest. The information provided by the images will be the same, except at different lightness. Voltage, though, changes the energy of the electrons, thus potentially affecting electron traps of different energies and providing a different information on the sample. All samples have thus been analysed at two different voltages: 2000 V and 4500 V.

For each sample pellet, several mosaics of approximately 6 x 6 mm² have been made at different exposition times and different voltages. Both sides of each pellet have been analysed. Each mosaic takes between 1 and 5 min to acquire depending on samples luminescence intensity, and between 4 and 7 mosaics were acquired per pellet face. With the addition of the time for vacuum pumping and electron beam stabilization (when changing its voltage) approximately one day of work is required for 8 samples. This time may be reduced once the data treatment is optimized and key conditions are clearly identified.

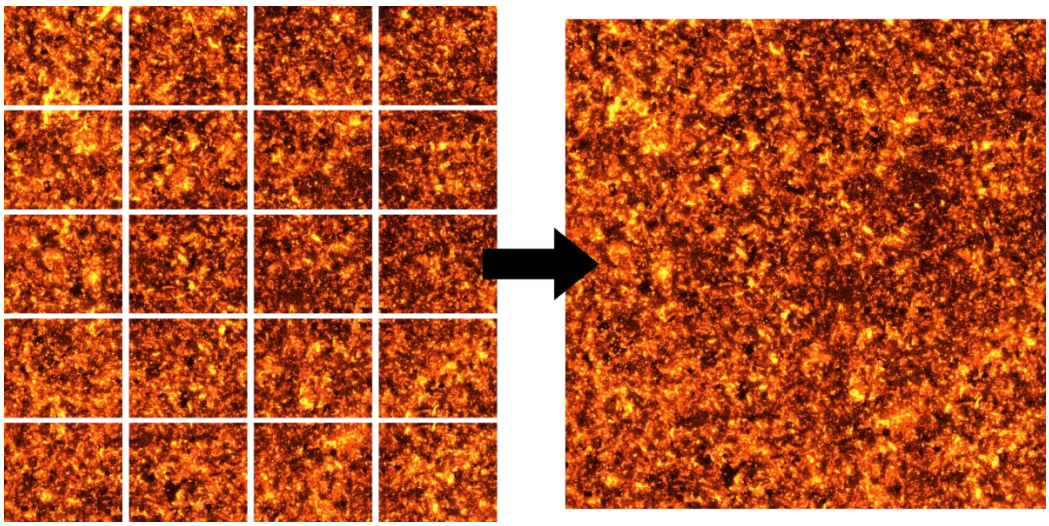

Figure 29: Example of the imaging of sample Li20 at 4500V with an exposition time of 100 ms. On the left, the raw images as saved by the Cathodyne software. On the right the reconstruct sample mosaic image. Spodumene, the Li-bearer mineral in this sample shows a bright orange to yellow luminescence.

Compared to the UV-bench, the scale of observation is much smaller (more details are visible like the presence of accessory minerals), and the analytical conditions are more adjustable. However, this versatility means the technique is also more complex to implement, and the time necessary for sample preparation and analysis makes this technique more time-consuming (while staying relatively quick).

3.2.2.3 Data treatment

One of the parameters we are the most interested in with UV-fluorescence and cathodoluminescence results is the colour, or more precisely the hue of the luminescence. Images retrieved from these analyses are provided in red, green and blue values (varying from 0 to 255). The information about hue is dependent of these three red, green and blue values. The first objective of this data treatment is to transform the red (*R*), green (*G*) and blue (*B*) values into another set of values, without losing or artificially adding any information, but grouping information on the hue within one parameter only (*H*).

Funded by the European Union

The hue refers to a colour independently from its lightness (*L*) or saturation (*S*) level. Saturation describes how bright a colour is, the lowest level of saturation being a grayscale when R, G, and B parameters have equal values. The maximum level of saturation is reached whenever at least one of the R, G, or B values is 0. The lightness of a colour is defined by its proximity to black (minimum lightness) or white (maximum lightness). The maximum lightness is reached when all R, G, and B parameters are at 255. The minimum lightness is reached when all R, G, and B parameters are at 0. The higher the sum R+G+B, the lighter the colour is. The hue being independent of the saturation and lightness, the full range of hues can be represented for a fixed saturation and lightness. Fixing saturation to 1 means the complete hue spectrum can be represented by only saturated colours, only defined by two values of R, G, and B (except for greyscale, here associated with black hue set to *H*=-1). Fixing the lightness finishes to constrain the possible R, G, B values necessary to cover the full hue spectrum (Figure 30).

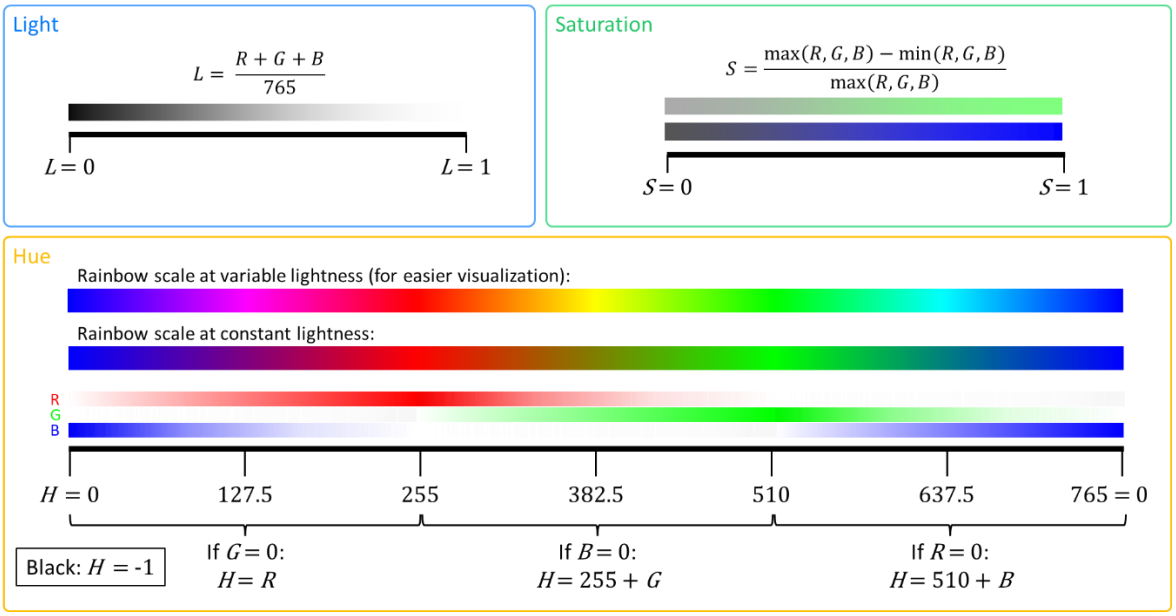

Figure 30: Light, saturation and hue system used for image treatment.

Analytical results are further treated as images with a hue (*H*), a lightness (*L*) and a saturation (*S*) value associated to each pixel.

3.2.2.4 UV-Bench results

General observations

A total of 68 samples has been imaged using the UV bench, including 41 spodumene samples (mostly concentrates), and 27 Li-mica samples (lepidolite and zinnwaldite).

Some luminescence variations, mostly intensity variations, are visible between samples. However, these visible variations do not seem to be related to the mineral type of the sample nor the Li-mineral concentration in the sample (Figure 31). Luminescence appears to be relatively homogeneous in most samples.

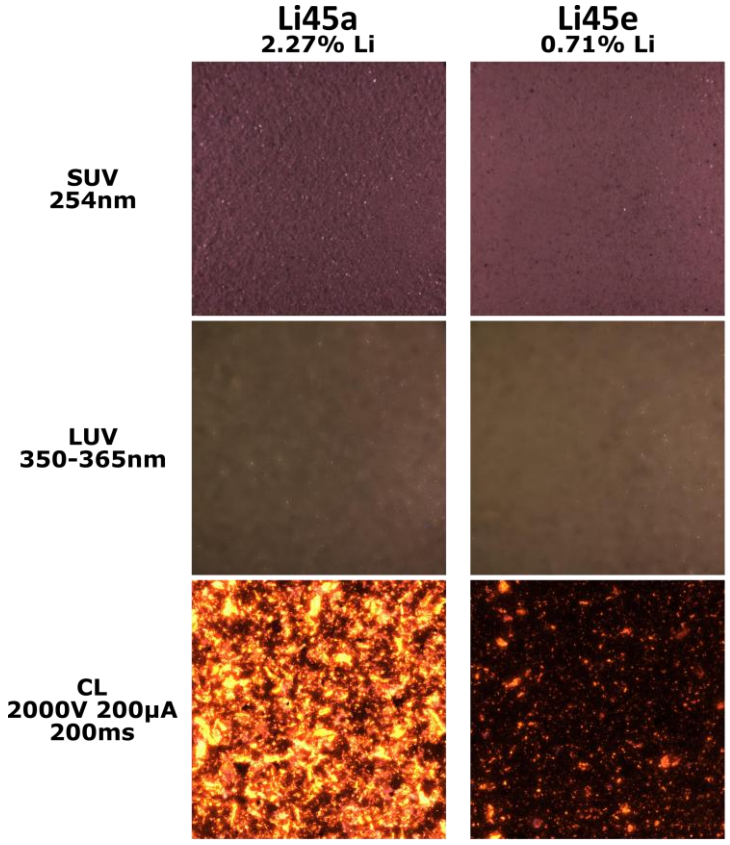

Figure 31: Example of spodumene sample luminescence for two samples of same origin but different spodumene (thus Li) concentrations. Remark the absence of remarkable difference for short UV (SUV) and long UV (LUV) luminescence, while the difference is obvious for cathodoluminescence (CL) where spodumene has an orange luminescence. UV images are ca. 3 cm width while CL images are 6 mm width.

Main results

UV images to be used for data treatment are cut to ca. 3 cm squares to remove the sample holder from the image. Treatment is only made on bulk image statistics since the luminescence is rather homogeneous in all samples and the image resolution does not allow to see many details.

We focused first on results based on samples hue. Results are provided in Figure 32 and Figure 33 for spodumene and Li-mica, respectively.

Funded by the European Union

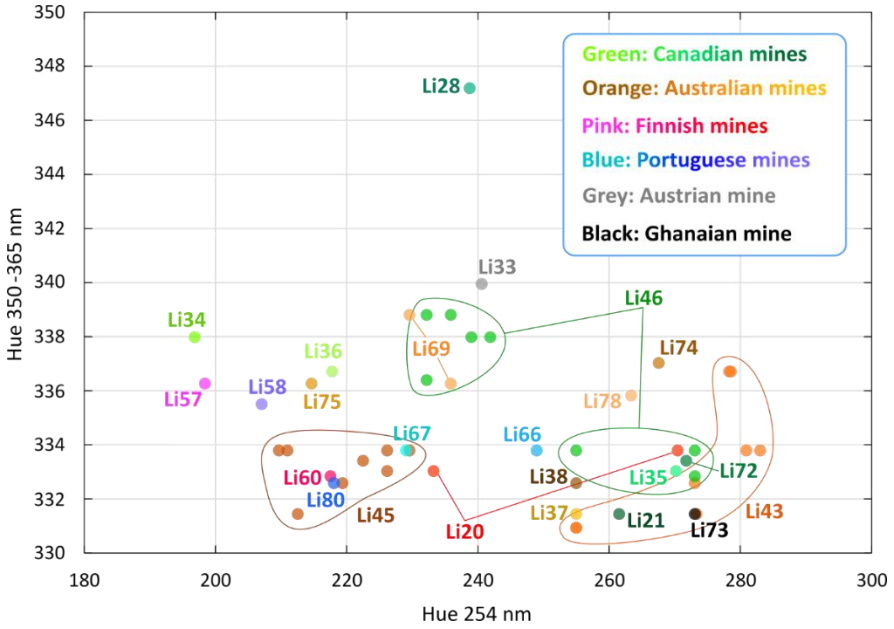

Figure 32: UV results based on hue for spodumene samples.

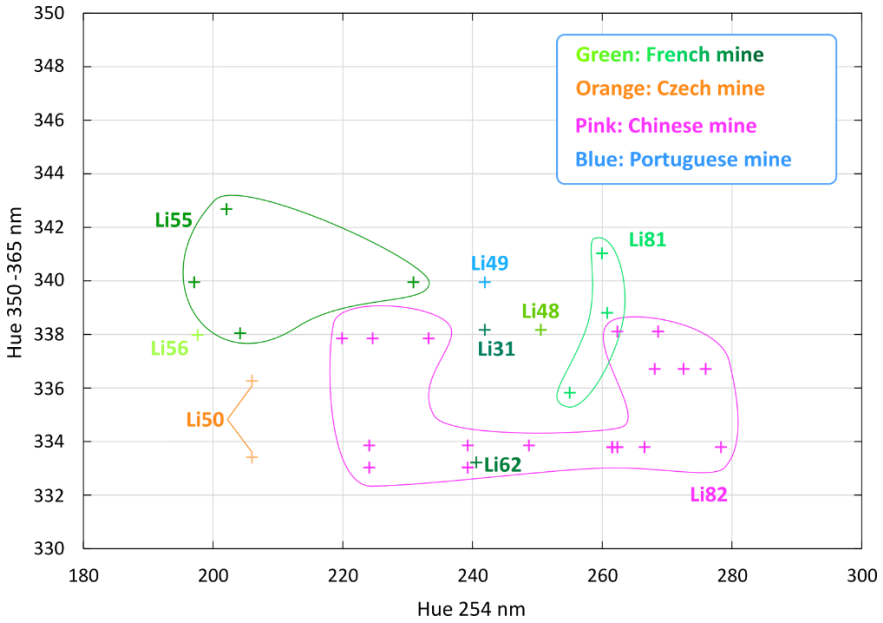

Figure 33: UV results based on hue for Li-mica samples.

While some samples groupments can be observed, the data spread and overlap between groups is pronounced. However, during the acquisition of these sample images, we noticed a fluctuation of the UV light intensity and decided to test its impact on the samples hue. Results of the tests made on sample Li20 (spodumene) are provided in Figure 34.

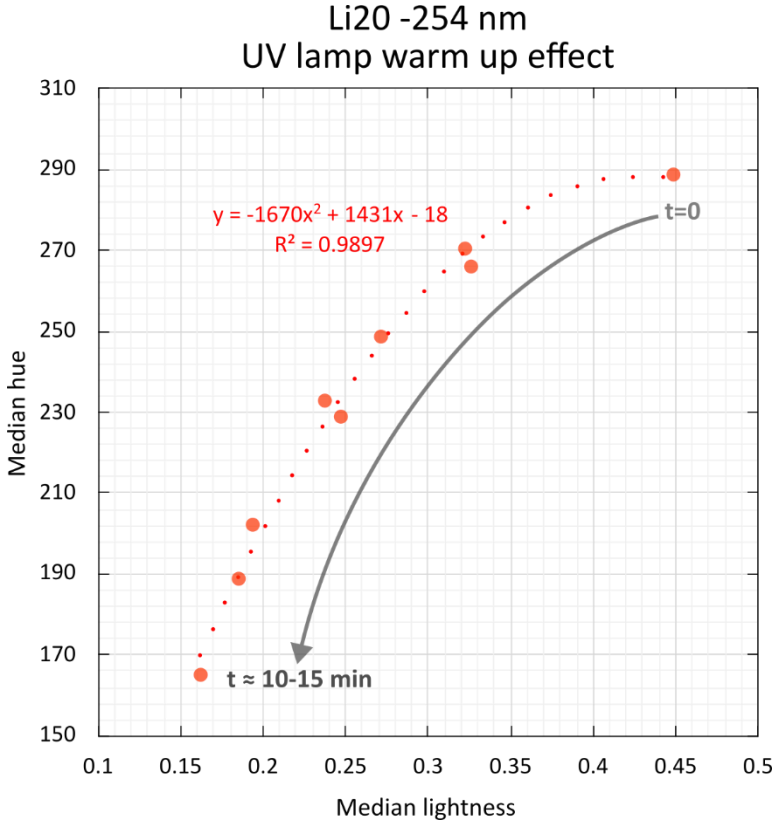

Figure 34: Temporal effect of the 254 nm UV lamp warm up on sample Li20 luminescence.

It shows a significant variation of the light source, impacting both the lightness and hue of the samples. This variation occurs in a relatively short time and certainly contributes greatly to the data spread observed in the hue results. It should be noted though that the UV source impact on lightness and hue is well defined by a quadratic relation. If this evolution is similar in every sample, it might be possible to correct for this light source deviation by record and correct the evolution of a reference sample during the acquisition session. Another option would be to replace the current UV sources with more stable light sources.

Outlook

Current results using the UV bench do not highlight a particular efficiency of the technique for traceability. However, the observed sample grouping, despite unstable UV light sources, indicates that the technique could benefit from further exploration with an improved setup or corrective approaches. Only then will the true potential of UV luminescence be properly assessed.

3.2.2.5 Cathodoluminescence results

General observations

A total of 95 samples has been imaged under the cathodoluminescence microscope, including 77 spodumene samples (mostly concentrates), and 17 Li-mica samples (lepidolite and zinnwaldite). Every sample has been imaged at least twice (both sides of a pellet). For a few samples, additional pellets were prepared to check the process repeatability.

Funded by the European Union

- There is a significant luminescence and colour difference between Li-mica and spodumene samples (Figure 35). Li-micas luminescence tends to be redder/pinker and is much less intense than spodumene luminescence. Moreover, the luminescence is more homogeneous over the sample surface in the case of micas than for spodumene.

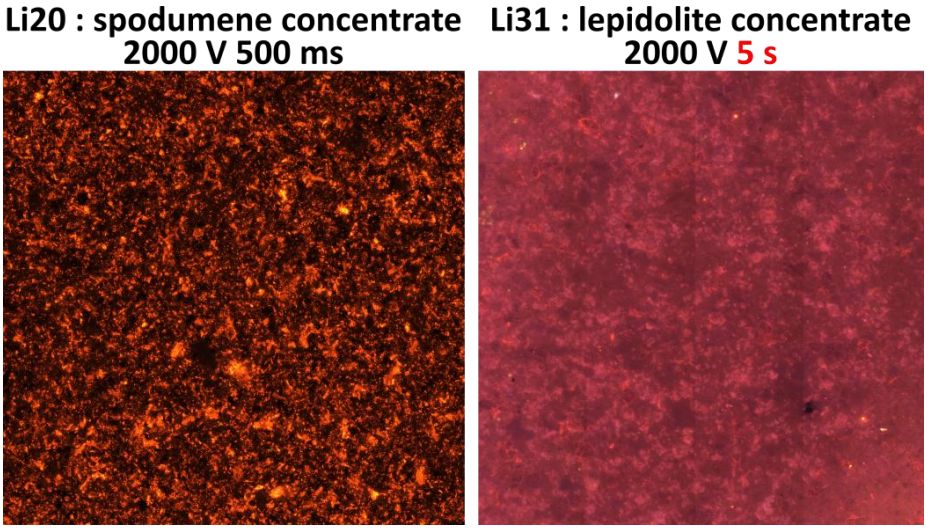

Figure 35: Comparison between spodumene (on the left) and lepidolite (Li-rich mica; on the right) cathodoluminescence. Notice the exposition time difference between the two images (500 ms vs 5 s). Images are 6x6 mm².

- Comparing different samples of spodumene from ore to pure spodumene, it can be observed that the spodumene concentration affects the amount of overall luminescence (Figure 36).
- There also are differences of luminescence intensity between spodumene samples of different origin (see the two spodumene concentrates examples on Figure 36). This difference is not solely due to differences in spodumene concentration.
- There seem to be slight colour differences between samples containing the same Li-rich mineral (see Li34 and Li21 in Figure 36 as an example). These colour differences may not always be obvious or even visible at a glance.

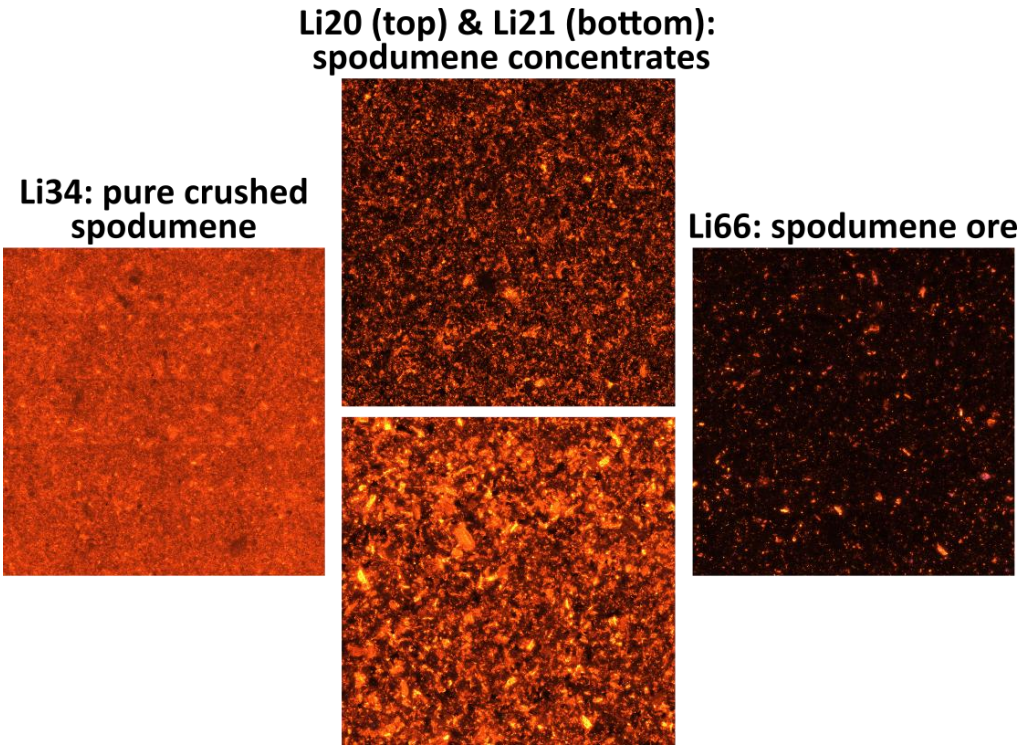

Figure 36: Cathodoluminescence comparison of different samples containing spodumene. All these images have been acquired in the same conditions at 2000 V and with an exposition time of 500 ms. Images are 6x6 mm².

- In ores and concentrates, there often are a few luminescent accessory minerals. These are most common and diverse in ore samples but can also be found in concentrates (Figure 37).

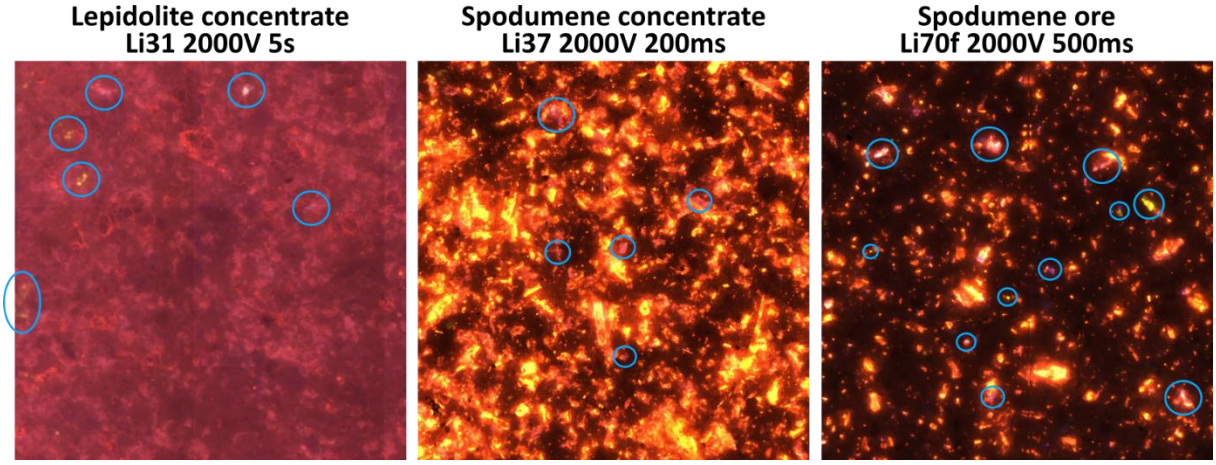

Figure 37: Luminescent accessory minerals in a few different samples (blue circles). Images are 3x3 mm².

Main luminescence results

Data treatment has been focused on spodumene samples as they were the most readily available and came from a wider variety of sources compared to Li-micas.

A mosaic of every spodumene sample (concentrates, ores and pure spodumene) has been made at 2000 V and 500 ms exposure time and at 4500 V and 200 ms exposure time so that results are comparable. In addition, a mosaic has been acquired at least at a second

Funded by
the European Union

exposure time for each voltage, adapted to the luminescence intensity of the sample. In general, spodumene concentrates have been imaged during 200ms at 2000 V, and during 50 ms at 4500 V, while ore samples have been imaged during 3 s at 2000 V, and during 1 s at 4500 V.

First observations highlighted the fact that, from one concentrate sample to another, the luminescence intensity and mineral proportion of low to no luminescence minerals is variable. As a first approach, we tried to compare the pixel lightness repartition between spodumene samples in given analytic conditions (Figure 38) as it should be sensitive to both luminescent mineral proportion and luminescence intensity. Using this method, ore samples stand out immediately as they are dominated by very dark pixels. Samples with a high proportion of spodumene such as sample Li34 (crushed large spodumene crystals) also stand out as their pixel lightness distribution is narrow and centered around mid-lightness values. Otherwise, among spodumene concentrates, it can be noted that samples from the same origin tend to have similar pixels repartitions. It is not true for all samples, which could be explained by different types of ore, or different mines within the same country. This may also reflect the technique and efficiency of the spodumene concentration process used by different operating companies.

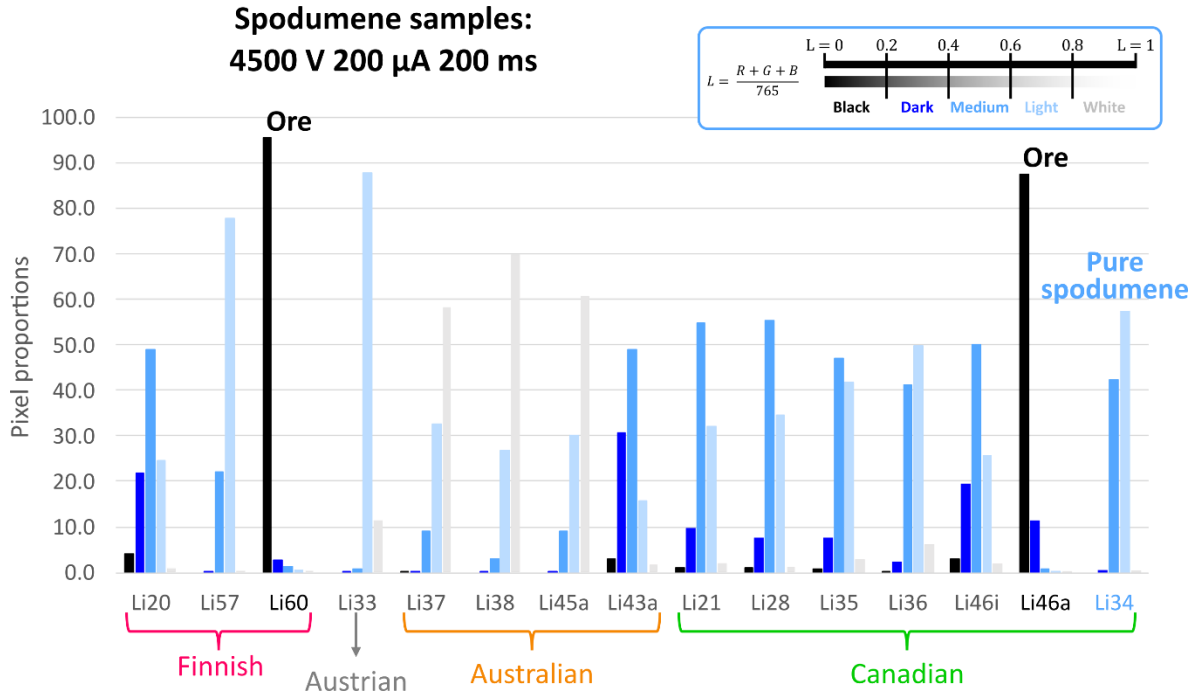

Figure 38: Results based on mosaic pixel lightness distribution for cathodoluminescence analyses made at 4500 V with an exposition time of 200 ms on spodumene samples (including two ores, and a pure spodumene sample). The majority of the samples are spodumene concentrates. For easier reading, a good diversity of analysed samples are shown here but not all of them.

A spodumene crystal under the cathodoluminescence electron beam should react in the same way whether it is contained within an ore or a concentrate sample. Thus, the luminescence intensity and colour of spodumene from the same origin, under the same analytical conditions, should be the same in a concentrate or an ore. The pixels characterization using hue, lightness and saturation should normally allow the direct comparison of all cathodoluminescence images as long as they have been acquired under the same voltage. However, luminescence intensity over- or under-saturation can impact the hue recorded by the optical camera. As an example, the orange spodumene luminescence

tends to turn yellow when the luminescence intensity becomes too strong for the camera. A solution can be to reduce the exposure time but the luminescence intensity of the different mineral grains in one sample is variable (for example due to internal reflections, microfractures, or internal variations in trace elements), and changing the exposure time will not make all luminescence variations disappear. The solution we choose to use is to select medium lightness pixels only and subsequently calculate the median hue of these pixels.

Using the fact that samples cathodoluminescence properties should vary with the applied voltage, we compare the median hue (of medium lightness pixels) obtained at 2000 V and 4500 V for all the imaged spodumene samples (Figure 39). To ensure the comparison is valid between the different samples, we only present results from images taken with the same exposure times but using this method should in theory allow to compare images of any exposure time (which has not been checked yet).

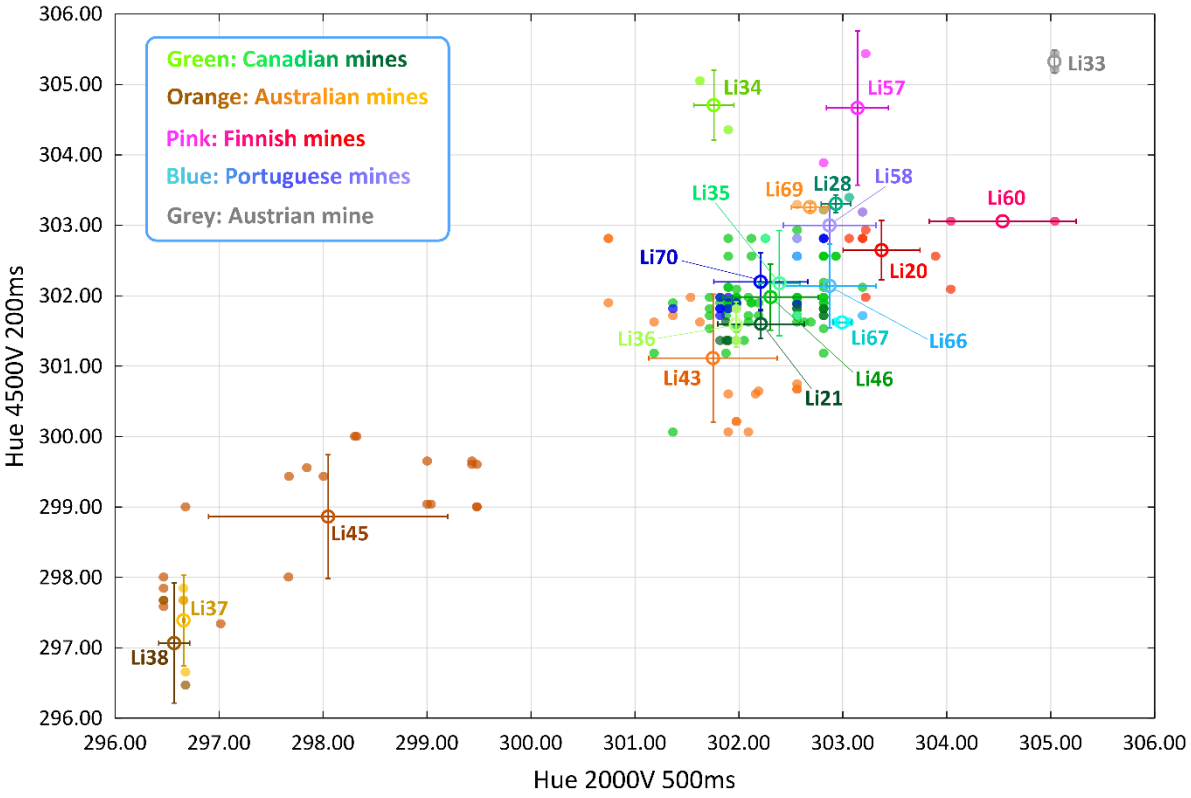

Figure 39: Samples hue at 2000V vs 4500 V with exposure times of 500 ms and 200 ms respectively. Full coloured dots indicate median hues (of medium lightness pixels) of individual sample images (i.e. there is one dot per imaged pellet face). Empty circles with error bars indicate the mean hue over one sample (averaging the values of all pellets faces) and its standard deviation. Canadian mines: Li21, Li28, Li34, Li35, Li36, Li46 ; Australian mines : Li37, Li 38, Li43, Li 45, Li69 ; Finnish mines : Li20, Li57, Li60 ; Portuguese mines : Li58, Li66, Li67, Li70 ; Austrian mine : Li33.

Results based on hue show a clear distinction of most Australian samples from Canadian and European samples. Sample Li33 from an Austrian mine is also clearly distinct from the rest of the results. The rest of the samples are relatively grouped. Canadian and Portuguese samples are completely undistinguishable but Finnish samples tend to have higher hue values.

Funded by the European Union

Use of accessory minerals

An interesting option for the traceability of Li-mineral concentrates is to use accessory minerals. Their presence, absence and proportions should vary from one origin to the other. The small pixel proportion represented by accessory minerals is however a challenge for their automatic identification and quantification. To get around this problem, we developed a pixel clustering approach (Figure 40). The first step is to filter out all the darkest pixels. Then a clustering method is used to group pixels with similar properties (hue, saturation and brightness). The approach to identify pixels with luminescent accessory minerals is to make the method create numerous groups so that even poorly represented groups are differentiated.

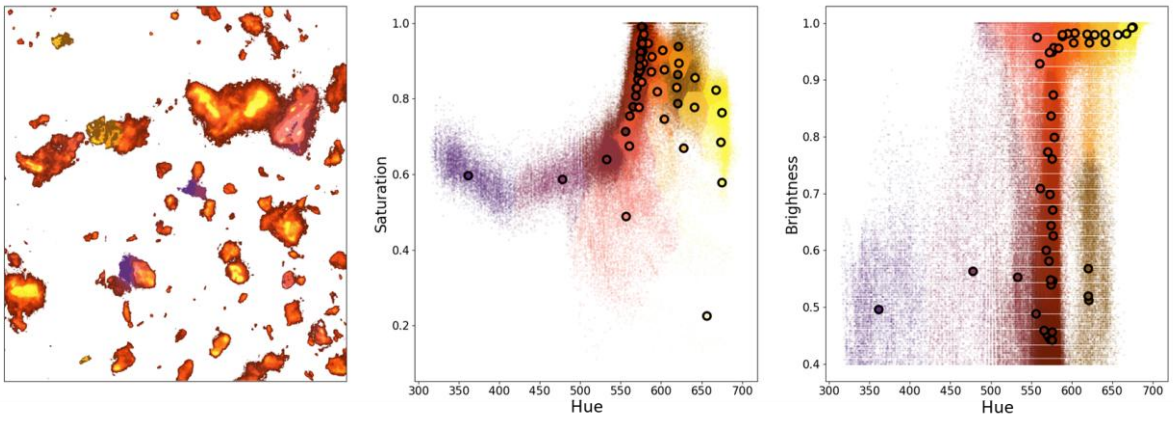

Figure 40: Clustering approach result on a 1 mm² zone of sample Li70f (spodumene ore). Accessory minerals with yellow, purple and pink luminescence colors can be identified. Dots with a black outline on the two figures on the right show the centroids positions of the different pixel clusters.

The next step will be to quantify the proportions and diversity of accessory minerals and then compare results from samples of various origins to check whether or not accessory luminescent minerals can be used for traceability.

Outlook

Initial results are promising. There is still considerable room for the improvement of the treatment method, especially on the use of accessory minerals, but also by combining results from various indicators such as the pixel lightness repartition and the median hue. The definition of a proper analytic procedure has to be done to optimize data acquisition and treatment.

All analyses presented here have been made on a single cathodoluminescence system, with the same camera. There is no doubt that the colors of the acquired cathodoluminescence images are dependent on the acquisition system. If this traceability solution was to be implemented on a larger scale, some kind of luminescent standard should be developed.

3.2.2.6 Method evaluation

The UV bench and cathodoluminescence were evaluated according to the five criteria defined in §2 Method evaluation (Figure 41, Table 5).

UV Bench

Mobility (M): The device is fully mobile and autonomous. It can work on batteries. The device is controlled by a tablet or a computer using Wi-Fi. The device is relatively sturdy but should be handled with a minimum of care due to the presence of the UV-lamps and camera inside. Based on these characteristics, a score of 9/10 is assigned.

Production Chain Coverage (PCC): This technique has been tested on ores and concentrates only. A score of 2/10 is therefore assigned.

Differentiating power (DP): We observe grouping of some samples of similar origin but also strong spread and overlap. The equipment used suffers from an unstable light source and the actual potential of the technique can only be assessed with an improved setup or corrective approaches. A score of 2/10 is assigned.

Cost of Implementation (COI): The production of the UV-bench prototype costed around 10 k€. This cost could be even lowered if the use of such device was generalized in the future. A score of 9/10 is assigned.

Operational Efficiency (OE): No sample preparation in the case of powdered samples. The analysis is extremely quick. Based on these advantages, a score of 10/10 is assigned.

Based on these scores and the defined weighting scheme, the resulting Global MFP Technic Index (GMTI) for the UV bench is 5.7, reflecting moderate overall suitability for traceability applications under the current configuration.

Cathodoluminescence

Mobility (M): This device requires a power supply, a computer and a table. The presence of optical parts requires a relatively clean environment. Moving it from one emplacement to another is possible but the device has not been built for this use. However, the building of a more portable version of the Cathodyne system does not seem to be impossible. Based on these constraints, a score of 6/10 is assigned.

Production Chain Coverage (PCC): This technique has been primarily used on Li-ores and mineral concentrates. NMC have been tested but showed no luminescence. A score of 2/10 is therefore assigned.

Differentiating power (DP): Results show the possibility to partially differentiate samples from diverse origins. Current results could be improved by further data treatment, especially focusing on accessory minerals. In the future, this technique may be even more promising and powerful thanks to the development of cathodoluminescence spectroscopy (today an exclusively laboratory technique). A score of 6/10 is assigned.

Cost of Implementation (COI): The Newtec Cathodyne system costs around 60 k€, to this can be added the cost of a classic optical microscope around 3 k€. A score of 8/10 is assigned.

Operational Efficiency (OE): Some preparation is required to obtain samples in pellet form. The necessity for the analysis to be done under vacuum and time required for the electron beam stabilisation slow down a little the analytical process. A score of 8/10 is assigned.

Funded by the European Union

Based on these scores and the defined weighting scheme, the resulting GMTI is 6.0, indicating a moderate to good overall suitability for traceability applications, with balanced performance but limitations in production chain coverage.

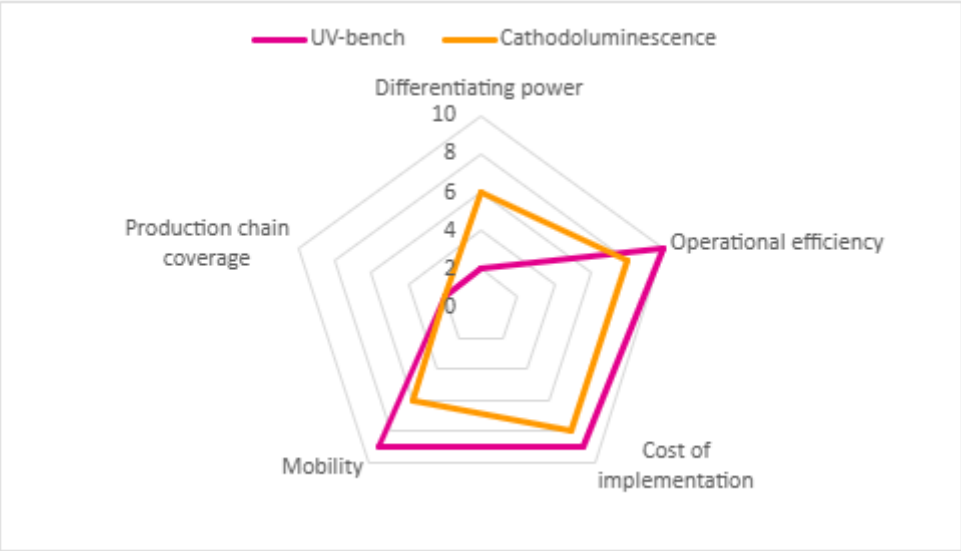

Figure 41: Method evaluation diagram for cathodoluminescence and UV-bench.

Table 5: GMTI score for UV-Bench and Cathodoluminescence.

		UV-Bench		**CL**	
Metric	Weight	Score	Weighted	Score	Weighted
DP	0.30	2	0.6	6	1.8
PCC	0.20	2	0.4	2	0.4
M	0.10	9	0.9	6	0.6
OE	0.20	10	2	8	1.6
COI	0.20	9	1.8	8	1.6
TOTAL (GMTI)			**5.7**		**6**

3.2.3 Methods based on X-ray fluorescence (XRF): handheld ED-XRF, mobile ED-XRF

3.2.3.1 Energy Dispersion X-ray fluorescence principle

The ED-XRF analysis is a non-destructive analytical technique based on the response of a sample to X-ray radiation. The emitted energy spectrum is characteristic of the sample's composition, with emission lines specific to the elements present and intensities proportional to their concentrations. Figure 42 shows the emission lines (Kα and Lα) specific to each element. In contrast to WD-XRF (Wavelength Dispersive X-ray Fluorescence), which separates X-rays by wavelength using diffraction crystals, ED-XRF (Energy Dispersive X-ray Fluorescence) detects all emitted X-ray energies simultaneously with a solid-state detector, enabling faster multi-element analysis with a simpler instrumental setup

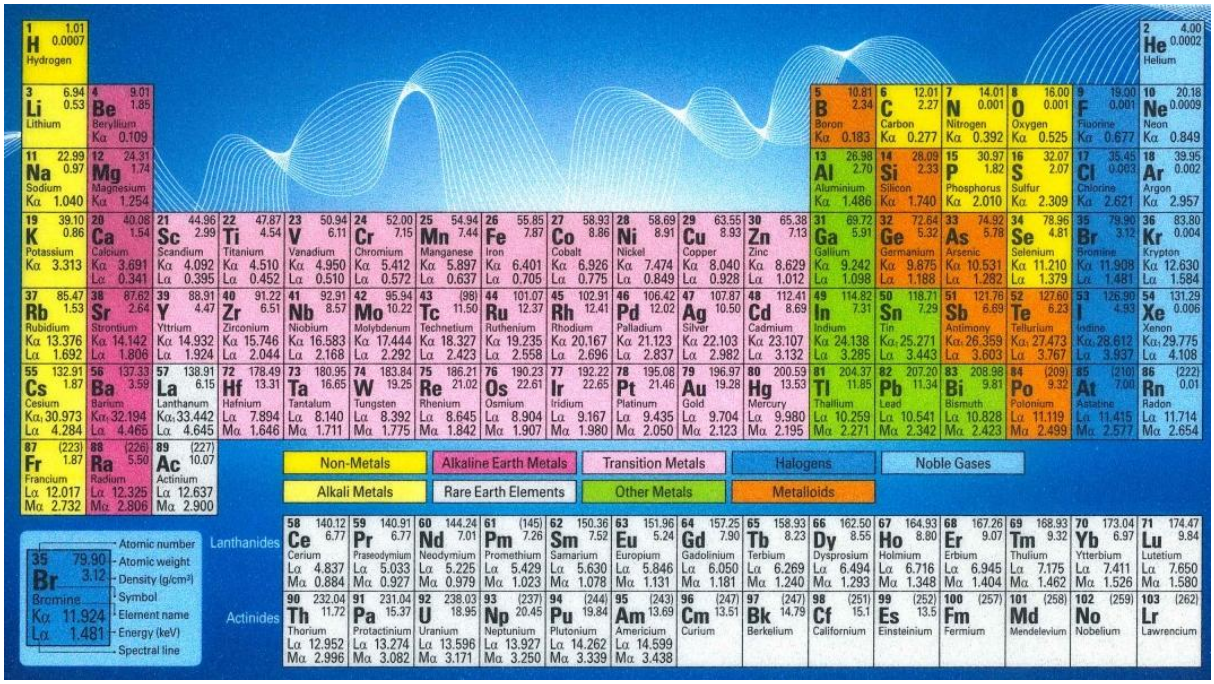

Figure 42: Characteristic emission lines of elements in the X-ray range.

3.2.3.2 Samples corpus and preparation, Instruments and data treatment description

A total of 93 samples from 14 different lithium deposit origins worldwide (Figure 1) were analyzed, along with 8 samples of unknown origin (see Table 1 for details). These samples include ores, mine concentrates, and intermediate processing products – such as rougher or cleaner flotation recoveries – referred to as pre-concentrates. The number of samples

Funded by the European Union

per deposit varies significantly, ranging from one to thirty-six. To minimize potential bias due to uneven sample coverage, the analytical approach was adapted accordingly.

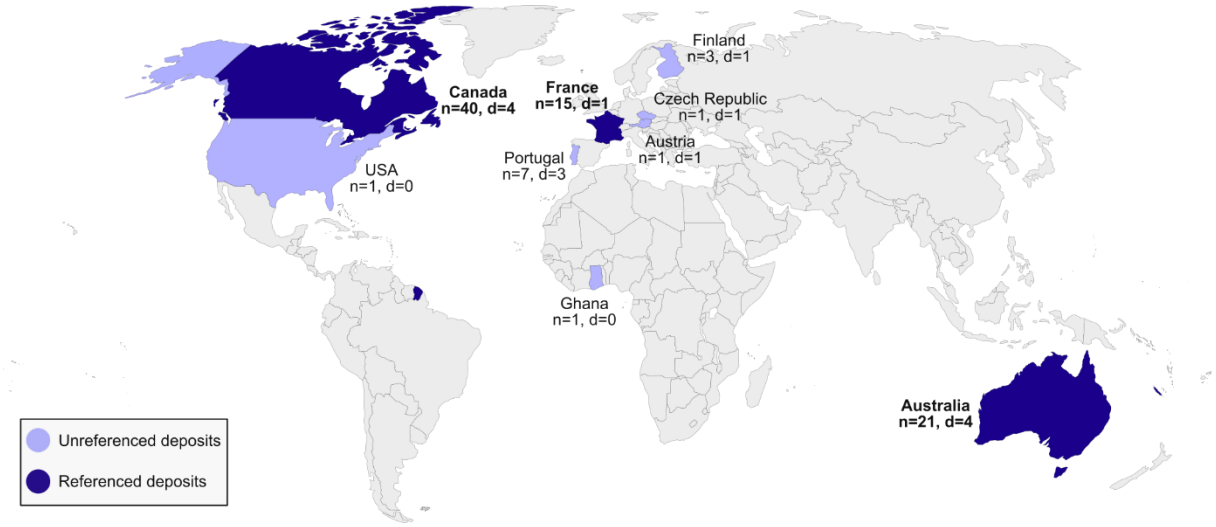

Figure 43: World map of the origin of samples used in this study. N= Number of samples. D=number of deposits/mines of known origin. In light blue, countries with unreferenced sample; in dark blue (and names in bold) countries with a referenced deposit (refer to data treatment for detail). (From Moradell-Casellas et al., in prep).

- *Sample preparation*

The sample bags provided by mine operators and sample providers were mixed, a quantity of approximatively 30g of sample was sampled and poured as it in XRF standard plastic cups on a 4 µm polypropylene film, for at least a two centimeters thickness in the cups.

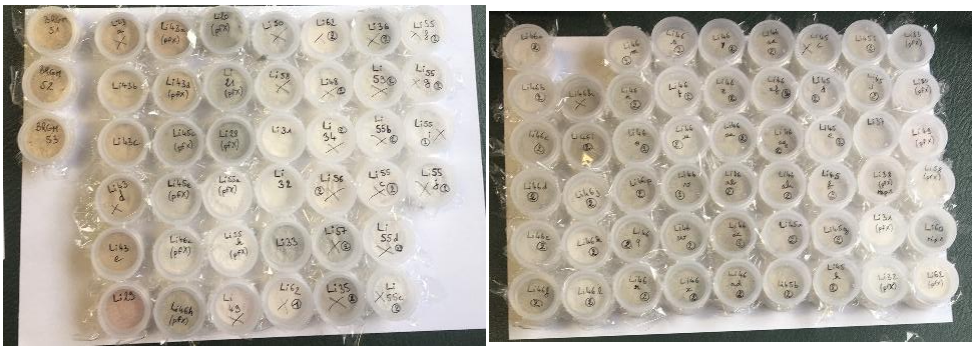

Figure 44: Samples cups with 4µm propylene film used for this study.

- Analytical protocol

This study uses three X-ray fluorescence (XRF) instruments: two portable spectrometers (pXRF) - the Hitachi X-MET8000 and the ThermoScientific XL3t980 Niton - and a mobile energy-dispersive spectrometer (mXRF) Ametek Spectroscout. Analyses were performed on the same samples prepared in cups to ensure comparability of results.

Handheld ED-XRF

Two pXRF instruments were used: the Niton XL3t-980 GOLDD and the Hitachi X-MET8000.

Both instruments were installed on their respective analysis stands to standardize measurements. Each sample was analyzed in all available modes, for a total time of approximately twelve minutes per sample per instrument.

The Niton is equipped with a 50 kV X-ray tube (100 µA, 2 W) with a silver anode and a large drift detector (LDD), analyzing a 50 mm² surface. The instrument was calibrated with the integrated silver target. Analyses lasted 30 seconds per filter (90 to 120 seconds total) using three or four factory-installed filters. Resolution ranges from 0.150 to 0.157 keV. Three analysis modes were used (Soil, Mining Cu/Zn/Pb, Mining Ta/Re/Hf), allowing measurement of 32 to 50 elements depending on the mode, by Compton normalization or fundamental parameters method.

The Hitachi X-MET8000 Expert has a 40 kV X-ray tube (50 kV in rare earth mode, 200 µA, 4 W) with a Rh anode and an SDD detector analyzing 100 mm². Calibration was performed with a 316 stainless steel reference. Analyses lasted 120 seconds with five filters, with time per filter automatically optimized. Four modes were used (Soil, Mining, Mining LE, REE), allowing measurement of 31 to 39 elements depending on the mode.

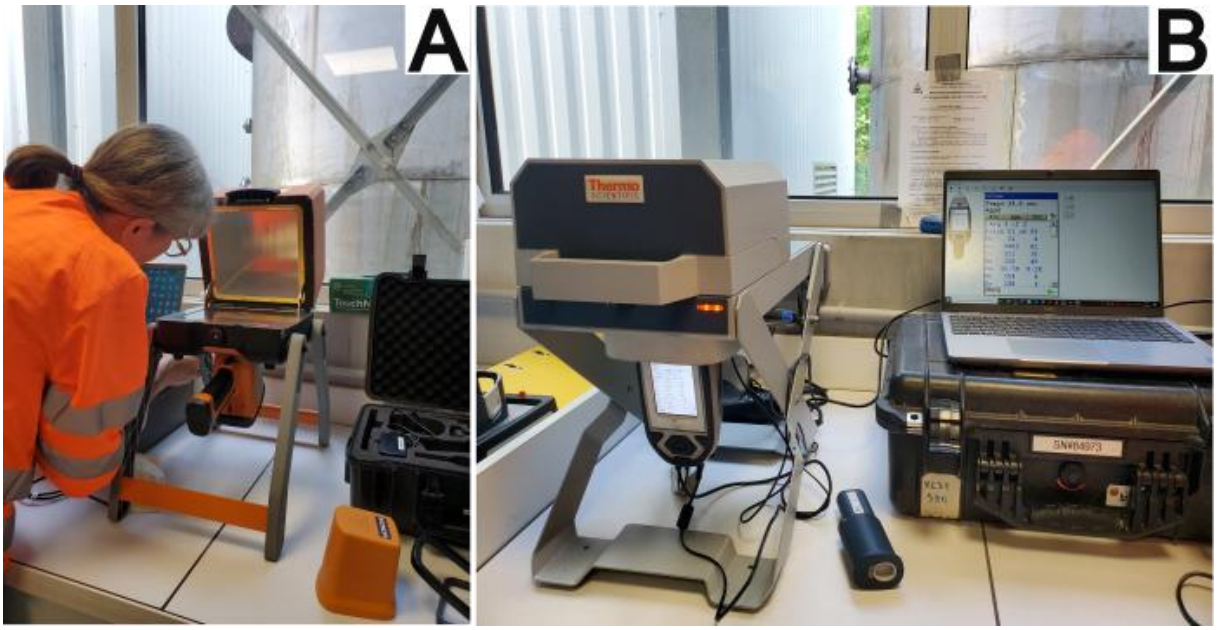

Figure 45: A) Hitachi XMET8000 installation on its stand, with protective case. B) Niton XL3t-980 GOLDD on stand during an analysis, connected to a portable computer for instantaneous data retrieving.

Mobile ED-XRF

The Ametek Spectroscout spectrometer is equipped with a 10 W X-ray tube (50 kV, Rh anode) coupled with a filter changer to optimize excitation of different elements. An integrated rotation system allows analysis of an enlarged sample surface (approximately 16 mm²). Analyses are performed under vacuum (<20 mbar) to improve sensitivity to light elements. Each sample is analyzed for a total of 15 minutes, with three measurements at different energies: 300 seconds at 11 kV, 300 seconds at 35 kV, and 300 seconds at 50 kV, each with filters optimized to detect light, medium, and heavy elements respectively.

Detection is provided by a large-area silicon drift detector (SDD), with a resolution below 155 eV (Mn K alpha) and a count rate reaching up to 200,000 counts per second. Calibration

Funded by the European Union

for major, minor, and trace elements was performed using a series of international reference materials (NIST, IRMM, USGS, CRPG, GBW, AMIS, SARM). Quantification is based on the manufacturer's geochemical method, combining spectral deconvolution, fundamental parameters, and Compton modeling.

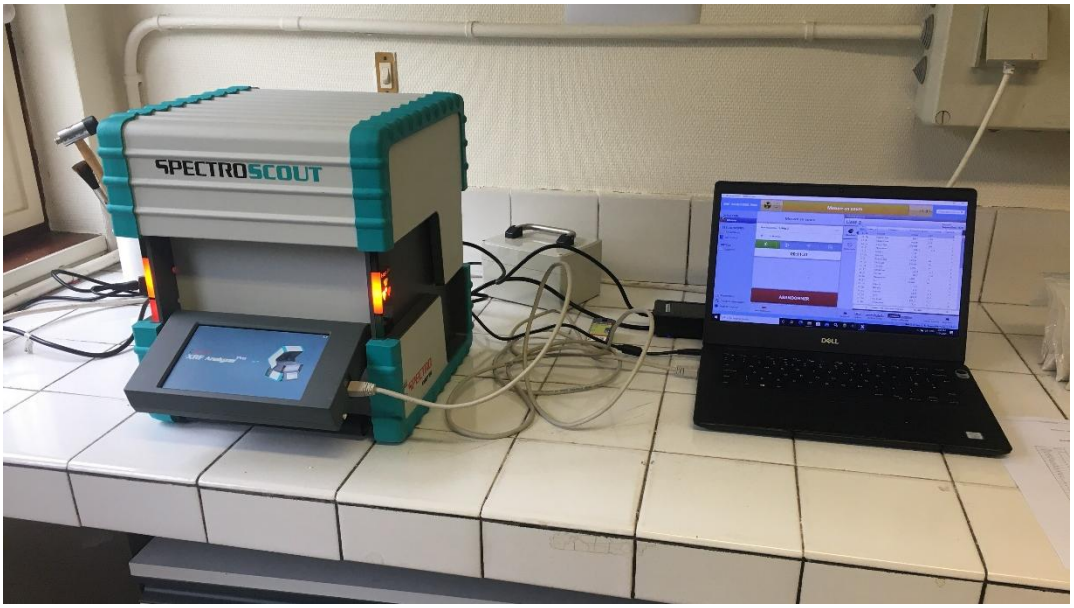

Figure 46: SpectroScout mobile ED-XRF lends by SpectroAmetek in BRGM laboratories.

- Data treatment

Based on the number of samples available and elements analysed and selected (explained later in the 3.2.3.3 section), we opted for a Linear Discriminant Analysis (LDA), which was optimized and modified for our specific needs and constraints. Further details on the methodology used are available and explained in the deliverable D2.5 and in a publication (Moradell-Casellas et al., in prep).

For the purpose of developing a robust and reliable traceability method, we have decided to use only deposits with ten or more samples to train the classification model. Three deposits were selected:

- A Canadian spodumene pegmatite (Canadian deposit "A", samples Ca-1 to Ca-36),
- An Australian spodumene pegmatite (Australian deposit "A", samples Au-1 to Au-12),
- A French lepidolite rare-metal granite (samples Fr-1 to Fr-15).

These will be referred to as reference deposits. All other samples and deposits, not used in model training, will be designated as unreferenced samples or deposits.

3.2.3.3 Results

- Detected elements and selection for data treatment

Detected elements in the samples are presented in Figure 47

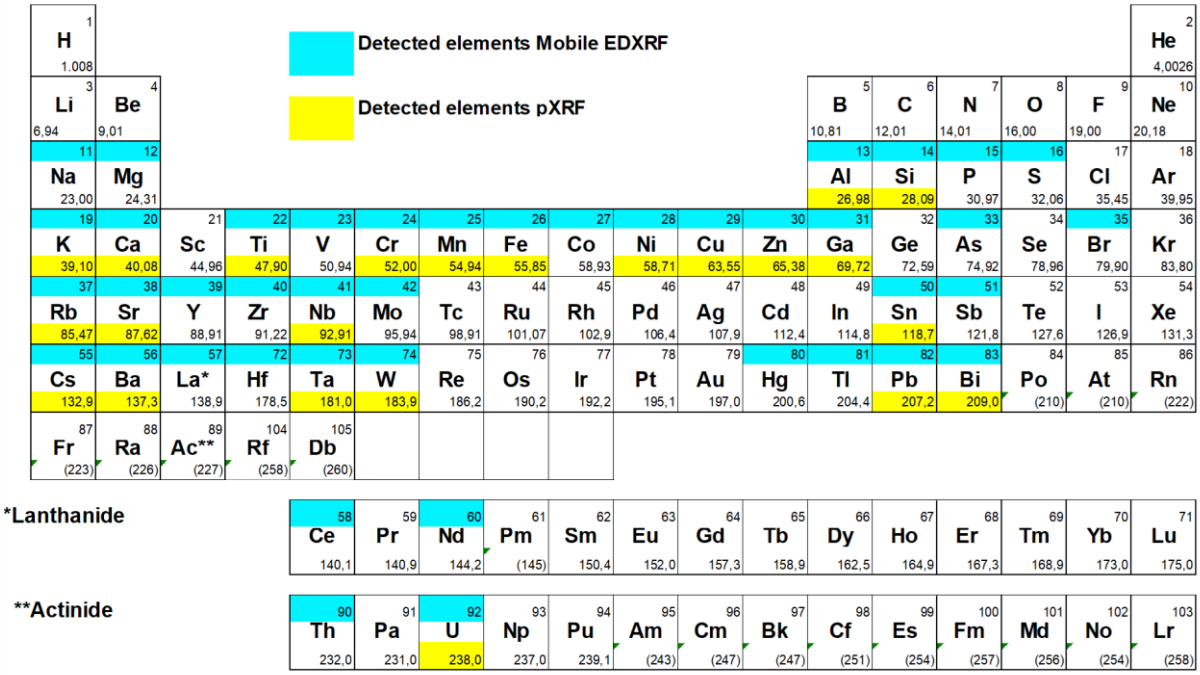

Figure 47: List of detected elements using pXRFs (in yellow) and mXRF (in cyan).

The elements analysed by the instruments included for the statistical treatment are first selected based on the detection limits. Elements where few (<5) or none of the samples exceeded the detection limit are not retained.

Furthermore, we selected elements based on accuracy by analysing standards in order to assess accuracy on these matrixes. As previously mentioned, The OREAS 999 standard has been used in that regard.

Funded by the European Union

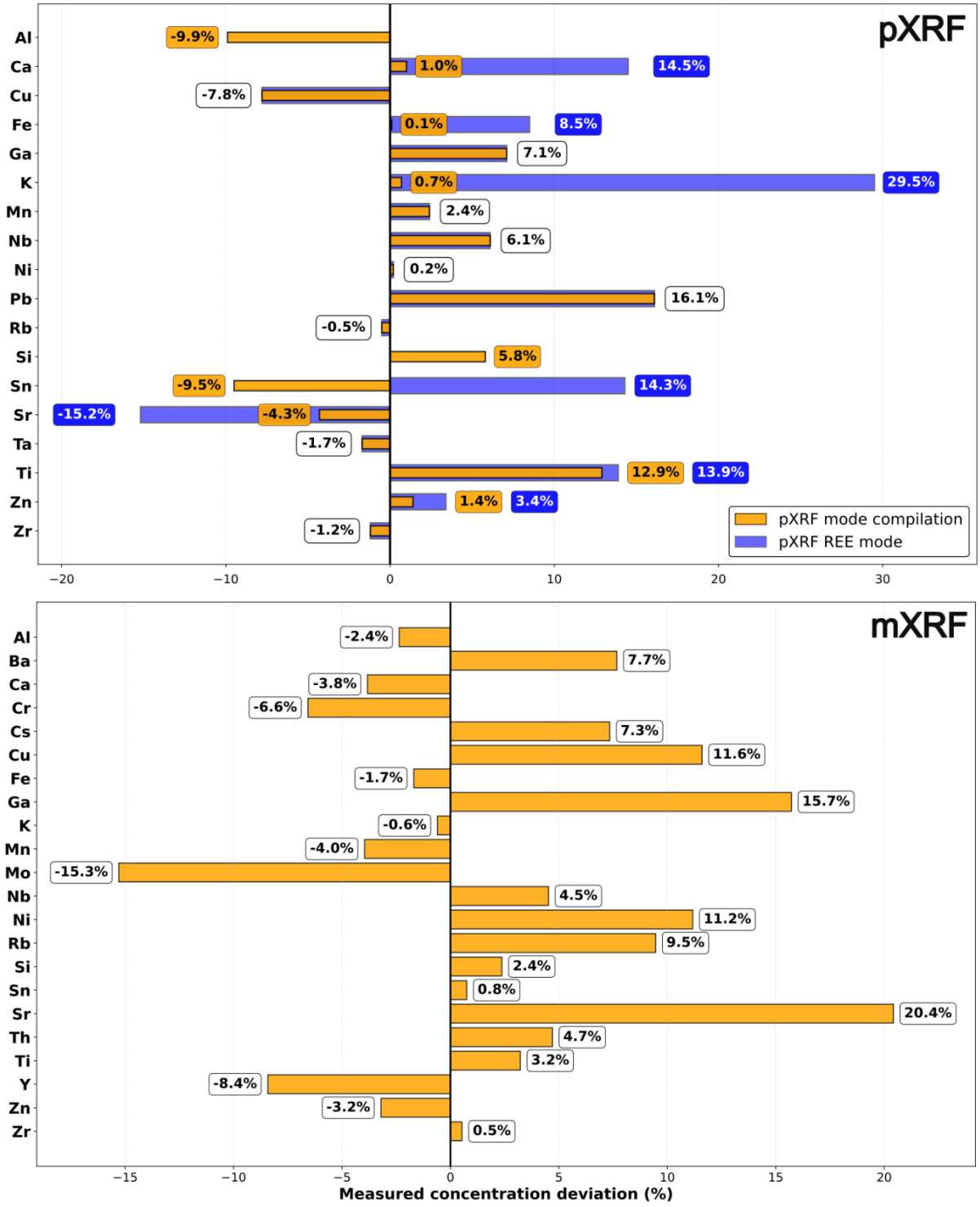

Figure 48: Concentration deviation of the measurement of OREAS 999 with mXRF and pXRFs to the certified values of the selected elements in percent. For pXRF, values in orange box stand for the compilation of modes, blue for the REE mode, values in white box correspond to the elements where REE mode was selected for the compilation (From Moradell-Casellas et al., in prep).

In the mXRF analysis: Al, Ba, Ca, Cr, Cs, Cu, Fe, Ga, K, Mn, Mo, Nb, Ni, Rb, Si, Sn, Th, Ti, Y, Zn, and Zr show measured concentrations that deviated by less than 20% from OREAS certified reference values, qualifying them for the data treatment. Sr is also kept because the measurement is close to the limit.

For pXRF measurements, element selection followed the same criterion: a maximum 20% deviation from OREAS 999 certified concentrations. Subsequently, the optimal analytical mode for each element was determined based on the accuracy of measurements compared to reference values.

Resulting mode chosen are presented in Table 6.

Table 6: Selected mode for the compilation based on analytical accuracy measurement of OREAS 999 concentrations.

Instrument	XMET8000			XL3t980	
Mode	Mining-FP mode	MiningLE-FP mode	REE-FP mode	Mining Cu/Zn/Pb mode	Mining Ta/Re/Hf mode
Elements	Ca, K, Ti, Zn	Si, Sr	Cu, Ga, Mn, Nb, Ni, Pb, Rb, Ta, W, Zr	Fe	Al

The REE-FP mode of the XMET8000 provides acceptable quantifications for most of the selected elements. As a result, this mode will now be considered independently. The same elements as in the compilation were evaluated, excluding Al, Ca, and Si, which are not analyzed in this mode. For all other elements (except for K, which is therefore excluded), the measured concentrations fall within ±20% of the certified reference values.

The selected elements for the three methods, the instruments limits of detection, and the mean concentration with observed ranges of the samples used for this study are presented in Figure 49: Mean concentrations of the samples in this study and limits of detection of selected elements in ppm for pXRF and mXRF, with observed concentration range of the samples. For compiled pXRF analysis, the detection limits of the selected modes were used. From Moradell-Casellas et al., in prep.

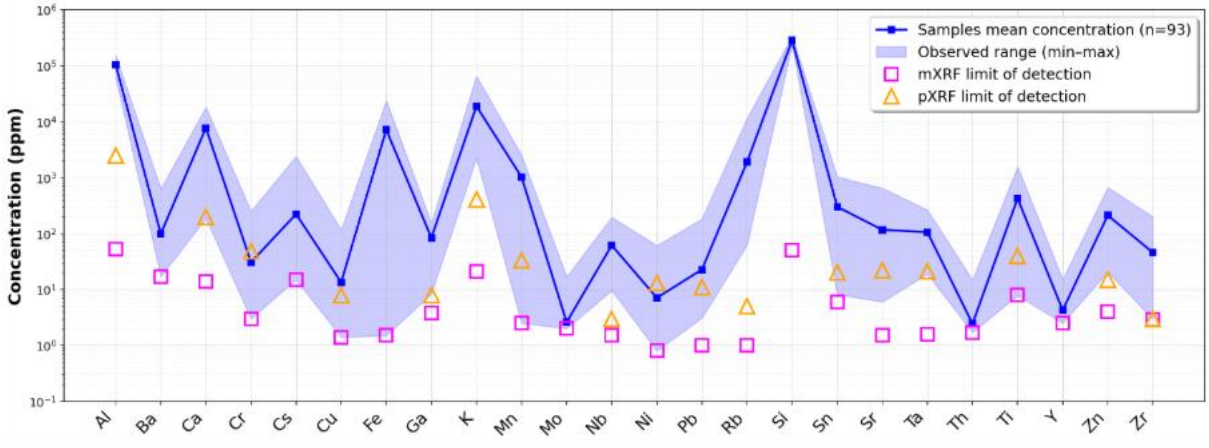

Figure 49: Mean concentrations of the samples in this study and limits of detection of selected elements in ppm for pXRF and mXRF, with observed concentration range of the samples.

Funded by the European Union

For compiled pXRF analysis, the detection limits of the selected modes were used. From Moradell-Casellas et al., in prep.

- Deposit discrimination and origin prediction

The latent space of the LDA for the three methods are presented in Figure 50.

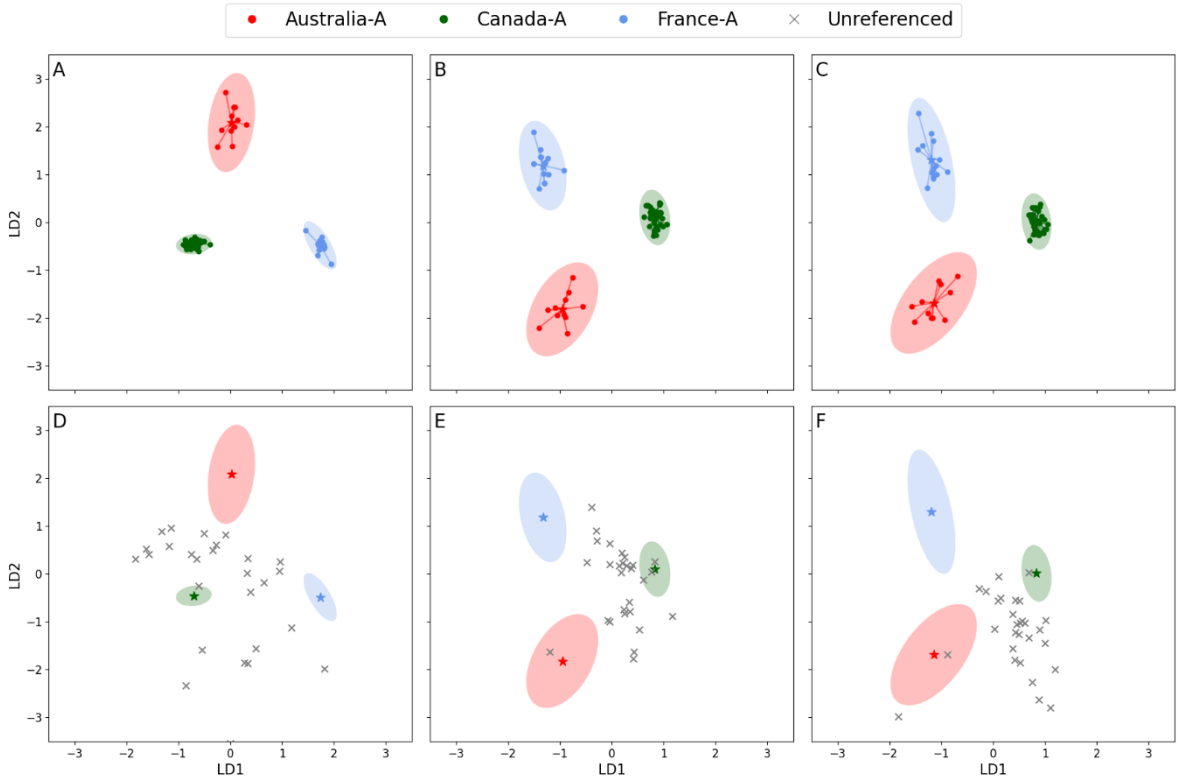

Figure 50: Projection of the samples belonging to the referenced deposits in the latent space built with LDA from the mXRF (A), pXRF compilation of modes (B) and pXRF REE mode (C) analysis. The samples belonging to unreferenced deposits have been projected in these latent spaces for comparison with the deposit centroids (stars) and their confidence region (D, E and F).

The trained model successfully separates the three reference deposits, with relatively small intra-deposit distances between samples. When projected into the resulting latent space, the unreferenced samples show large distances from the reference deposits—except for the Canadian deposit that overlaps in the three models with one (two in the compilation) unreferenced sample.

We ran predictions of sample provenance with a leave-one-out cross-validation (LOO-CV) approach, modified and presented in the deliverable D2.5 and in Moradell-Casellas et al. (in preparation); in order to demonstrate how the presented approach could verify the origin of the samples from the three reference deposits, and reject other samples. The resulting confusion matrix is shown in Figure 51.

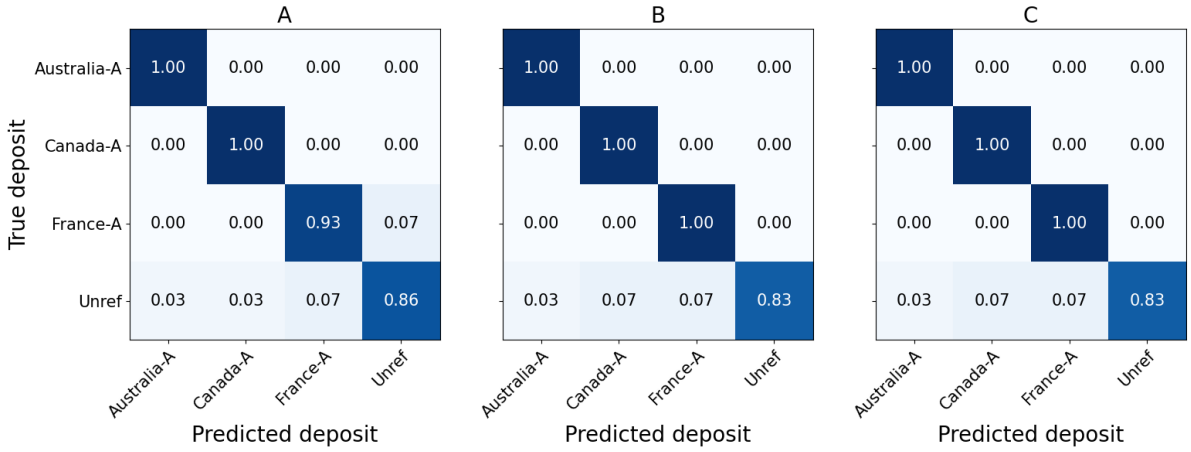

Figure 51: Confusion matrices of the LOO-CV resulting from models trained with mXRF (A), pXRF (B) and pXRF_REE (C) datasets. Anonymized samples from the Australian deposit (Au_A), the Canadian deposit (Ca_A) and the French deposit (Fr_A) were used for model training and the unreferenced samples were also used for prediction. A prediction score of 1 between True and Predicted deposit would be a perfect compliance between true origin and predicted one, whereas 0 would be a total discrepancy between them. From Moradell-Casellas et al. (in preparation).

The results show perfect classification accuracy for samples from the Australian and Canadian reference deposits. For the French deposit, the mXRF model incorrectly rejects one sample. However, the pXRF models correctly classify this sample as belonging to the French deposit.

The rejection of unreferenced samples averages a score of 0.83% for the pXRF, and a slightly better result with mXRF of 0.86%. False positives are attributed to the three referenced deposits. Nevertheless, the details regarding the origin of these samples provide some context and explains the reasons behind these errors. More details in Moradell-Casellas et al. (in preparation).

3.2.3.4 Method evaluation

The pXRF and mXRF were evaluated according to the five criteria defined in §2 Method evaluation (Figure 52, Table 7).

pXRF

Mobility (M): Although the devices are used on stands in this work, they are equipped with a battery that enables handheld analysis in the field. They can be packaged in protective cases for easy transportation. A score of 9/10 is assigned.

Production Chain Coverage (PCC): The results presented in this work only cover the upstream of the supply chain, from mine ore to mineral concentrate. The capabilities of these instruments in terms of limit of detection make it impossible to analyze trace elements in further steps. A score of 2/10 is therefore assigned.

Funded by the European Union

Differentiating power (DP): The prediction of origin is nearly perfect, with high True Positive Rate which allow to certify the provenance of reference deposits. A score of 9/10 is assigned.

Cost of Implementation (COI): The prices for pXRF vary from 20k to 50k€, the analysis does not entail any significant additional costs. The level of human training required is minimal. A score of 9/10 is assigned.

Operational Efficiency (OE): This method allows a rapid and direct analysis of the samples; however, the X-Ray source requires safety measures. A score of 9/10 is assigned.

Based on these scores and the defined weighting scheme, the resulting GMTI is 7.6, indicating a high overall suitability for traceability applications, particularly for upstream stages of the value chain, despite limitations in trace-level detection for more advanced processing steps.

mXRF

Mobility (M): This device is equipped with a battery that enables analysis in the field. They can be packaged in protective cases for easy transportation. A score of 9/10 is assigned.

Production Chain Coverage (PCC): The results presented in this work only cover the upstream of the supply chain, from mine ore to mineral concentrate. However, the capabilities of this instrument in terms of limit of detection make it possible to analyze trace elements in cathode active materials, maybe up to the battery. A score of 4/10 is therefore assigned.

Differentiating power (DP): The prediction of origin is nearly perfect, with high True Positive Rate which allow to certify the provenance of reference deposits. A score of 9/10 is assigned.

Cost of Implementation (COI): The prices for mXRF are typically around 50k€, the analysis does not entail any significant additional costs. The level of human training required is minimal. A score of 9/10 is assigned.

Operational Efficiency (OE): This method allows a rapid analysis of the samples prepared in cups; the X-Ray source requires safety measures, they are nevertheless equipped with shielded enclosure. A score of 8/10 is assigned.

Based on these scores and the defined weighting scheme, the resulting IGMTI is 7.8, indicating a high overall suitability for traceability applications, with strong performance across most criteria and extended potential along the value chain compared to pXRF.

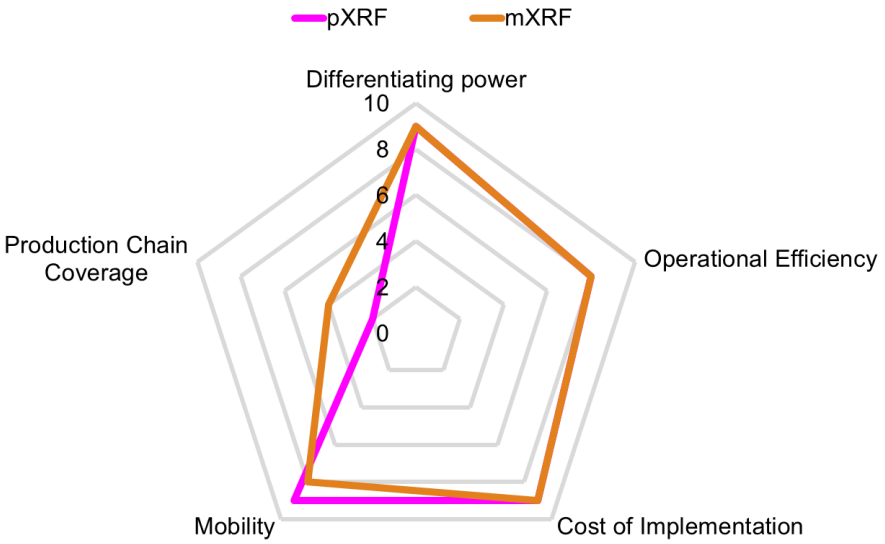

Figure 52: Method evaluation diagram following the 5 criteria for pXRFs and mXRF.

Table 7 : GMTI score breakdown for pXRFs and mXRF.

		PXRF		**mXRF**	
Metric	Weight	Score	Weighted	Score	Weighted
DP	0.30	9	2.7	9	2.7
PCC	0.20	2	0.4	4	0.8
M	0.10	9	0.9	9	0.9
OE	0.20	9	1.8	8	1.6
COI	0.20	9	1.8	9	1.8
TOTAL (GMTI)			**7.6**		**7.8**

Funded by the European Union

4 Methodology for on-site material flow characterization along the battery production chain: natural graphite

4.1 Leverage points

Natural graphite is mined and physically processed (grinding and flotation) in multiple stages, thereby increasing graphite contents from ca. 10-30% to over 90%, before it is sold as a graphite concentrate. Given the low value of graphite ore compared to graphite concentrate and the simplicity of physical processing, no long transport of graphite ore is expected, while processing raw ore from various nearby mining operations (i.e., on-site mixing) can potentially occur to some extent. The first major leverage point in the graphite processing chain is therefore at the concentrate level. In 2023, approximately 73% of global natural graphite production took place in China (Reichl & Schatz, 2025). On the other hand, chemical purification takes place almost exclusively in China. The second major leverage point of the graphite production chain is therefore after the chemical purification stage.

Based on the results obtained by laboratory techniques on natural graphite products, graphite flakes are intermixed with various types of minerals from raw ore down to the highest purity stages at the value chain. The specific suite of these minerals is characteristic for the individual deposits and therefore their analysis provides a means for natural graphite traceability (Arató et al., 2025). Hence, the key aspect in the characterisation of on-site natural graphite characterisation also preferably focuses on the precise detection of mineral impurities or their chemical signature corresponding to chemical heterogeneities in graphite products.

4.2 Selected techniques

The most straightforward mobile techniques for the chemical analysis of geological materials are XRF and LIBS and we tested both techniques accordingly, while our primary focus was on LIBS.

4.2.1 Handheld LIBS

4.2.1.1 Method description

The sample set dominantly comprised physically purified (grinding and flotation) samples, but also chemically purified specimens, including two-step-base and base-acid-purified samples. For the analysis of natural graphite, we utilized a SciAPS Z-903 handheld LIBS instrument (Figure 53). This instrument operates with a solid-state laser at 1064 nm wavelength, 5-6 mJ energy, 50 Hz frequency and Argon plasma. The plasma is generated directly at the sample surface while the exit slot of the instrument (Figure 53) is covered by the sample and the laser is ignited. Our instrument was set up to ablate 7*7 rectangular spots, resulting in a ca. 1x1 mm ablated surface. For the purpose of the measurements, pressed pellets were prepared from graphite concentrates with 2-3 mm thickness and 32 mm diameter. 10 areas were ablated on each pellet. Each area was ablated 49 times, resulting in one average spectrum per area. Where enough material was available, two pellets were prepared from the same sample, and 10 areas were analysed on each pellet. This approach was meant to ensure that the spatial heterogeneity is captured within the

Funded by the European Union

samples, and the analyses are representative. Normalized intensities were used for the numerical evaluation of the data. Normalized intensities were calculated by dividing raw intensities at each wavelength by the total intensity of the spectrum. This step is necessary to ensure comparability between individual measurements as LIBS is an optical technique, where the exact position of the sample and surface characteristics can significantly modify raw intensities.

For independent control measurements, Instrumental Neutron Activation Analysis was performed at the Technical University of Vienna. For elements where INAA is limited by high detection limits (e.g., K, Mg), data from the same samples obtained by solution ICP-MS or laboratory XRF was used for comparison (see also Deliverable 2.4. for further details about laboratory methods). Carbon contents were independently determined by thermogravimetry.

Figure 53: SciAps Z903 handheld LIBS instrument used for the analysis of natural graphite.

4.2.1.2 Results

The visual inspection of spectra reveals that there are significant differences between individual deposits (Figure 54), owing to their different mineral contents, with comparably smaller variance between samples from the same deposit but different production year.

Funded by the European Union

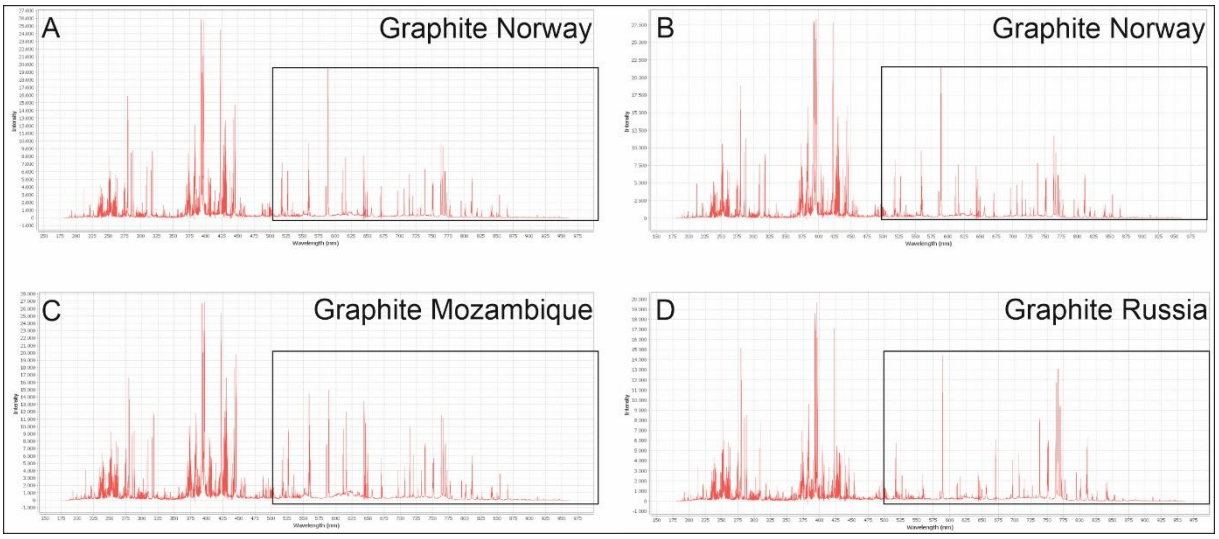

Figure 54 : Typical handheld LIBS spectra of graphite concentrates. Wavelength is presented on x-axis while intensity is shown on the y-axis. Highlighted areas show noticeable differences between different countries and almost identical spectra for the two samples from Norway.

An extensive set of individual emission lines for 22 elements were extracted from the combined data table of all analyses, initially comprising over 8000 wavelengths. In Figure 55, relative intensities averaged for 10 areas/sample are plotted against concentrations determined by independent methods, with the result of linear regression performed on the comparative dataset. Al, Ca, Cr, Fe, K, Mg, Mn, Na, Si and V show an R^2 value of at least 0.6, implying that the concentrations of these elements and their corresponding wavelengths reflect true concentration changes in the samples.

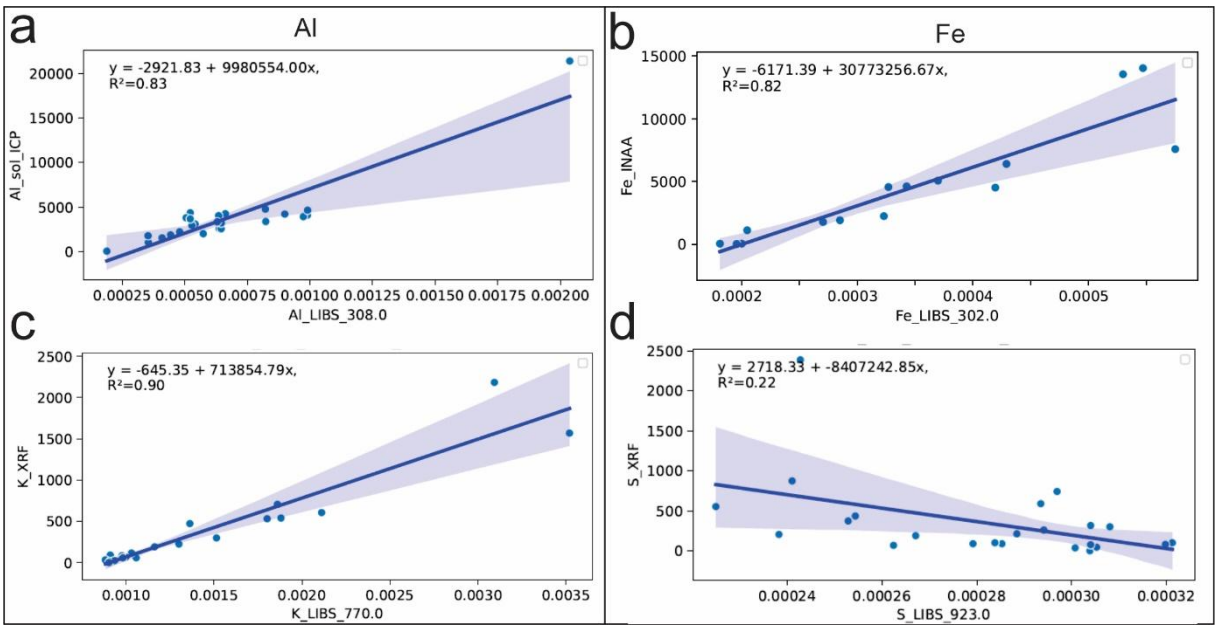

Figure 55: Relative handheld LIBS intensities compared with results from independent methods (in ppm). a-c: LIBS relative intensities reflect independently determined concentrations d: LIBS fails to detect sulphur in the studied samples despite high concentrations.

According to the above list of quantifiable elements, the data table was filtered to their corresponding wavelengths, while other elements were left out from further data analysis, as their corresponding signal intensities would only contribute with noise to the dataset.

Funded by
the European Union

This filtering results in a set of 27 variables. The approach is not finalized yet as several elements (e.g., H, N, O) can also potentially contribute to the differentiation but their concentrations were not independently analysed yet.

Random forest classification was performed on four deposits, where samples from multiple years were available (Brazil: 6, Mozambique: 7, Norway: 4, Ukraine: 3). For this purpose, results of individual areas (10 for each sample) were considered. Cross-validation was performed with the GroupKFold approach, meaning that in each iteration the data from one sample from each deposit was entirely excluded from training and used for testing. This conservative approach yields an overall classification score of 80% (Figure 56). The overall score is significantly lowered by the small number of available samples for Ukraine and the considerable year-by-year variation in the Mozambique samples. Overall, the results imply that unknown graphite concentrates can be correctly classified based on handheld LIBS data, if a comprehensive reference database (i.e., from many different years and parts of each deposit) is available for each deposit in the future.

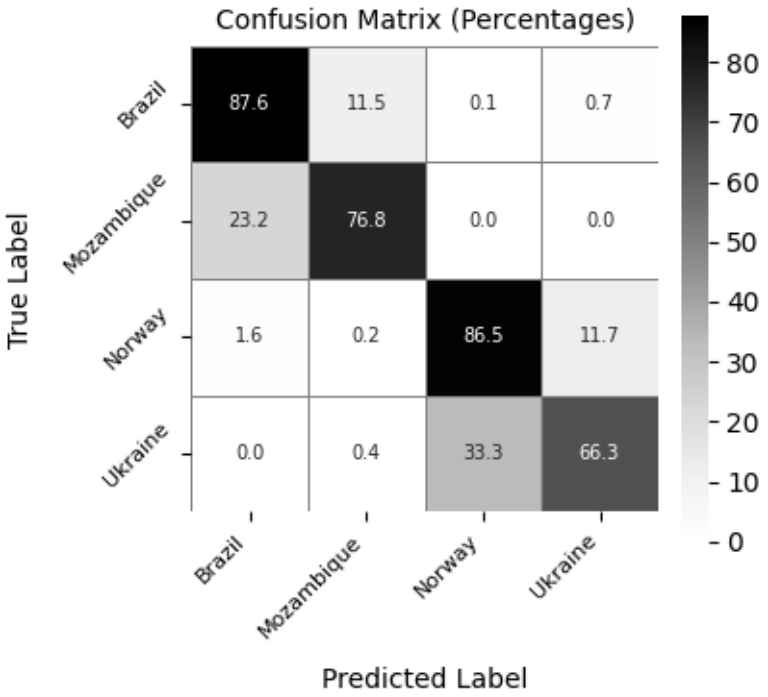

Figure 56: Confusion matrix of graphite concentrates based on random forest classification.

4.2.1.3 Technique assessment/Method evaluation

The handheld LIBS is evaluated according to the five criteria defined in §2 Method evaluation (Figure 57, Table 8).

Mobility (M): Handheld LIBS excels at mobility as the instrument can be transported in a suitcase and also utilized on the field or production environments A score of 10/10 is assigned. (Mobility: 9/10).

Operational Efficiency (OE): It also excels at operational efficiency as only a few tens of seconds are needed for one analysis once the system is set up, while data export can be tedious with this specific instrument and pellet pressing also needs extra effort. Therefore, a score of 8/10 is assigned.

Funded by the European Union

Cost of implementation (COI): The instrument ranks also high in terms of cost (i.e., low cost), its market price being significantly lower than any of the laboratory instruments discussed in deliverable 2.4. A score of 8/10 is assigned.

Differentiating power (DP): Due to the extensive set of simultaneously measured major and minor elements, its differentiating power is high, while the instrument is not suitable for measuring trace and several minor elements in the samples in contrast to several laboratory techniques. Less available parameters compared to those techniques mean a less efficient multivariate classification. Therefore, a score of 7/10 is assigned to the technique in this respect.

Production chain coverage (PCC): The limited sensitivity to trace elements restricts the applicability of the method at advanced stages of the value chain. In chemically purified samples, only light elements such as C, H, O, and N can be detected, which significantly limits traceability potential. A score of 4/10 is therefore assigned.

Based on these scores and the defined weighting scheme, the resulting Global MFP Technic Index (GMTI) is 7.0, indicating a high overall suitability for traceability applications, particularly for rapid, on-site analysis, despite limitations in trace element detection at advanced processing stages.

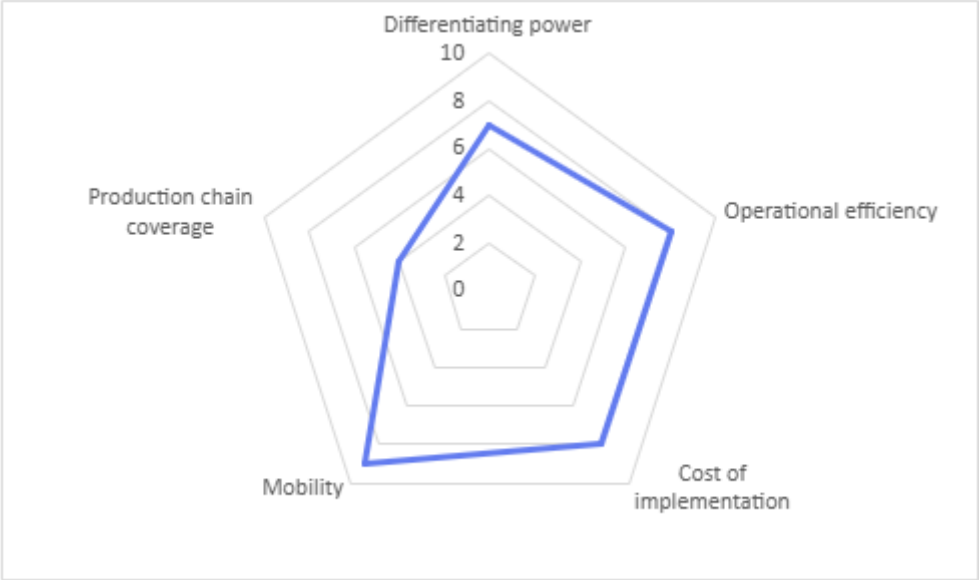

Figure 57: Method assessment of the handheld LIBS instrument.

Table 8 : GMTI score breakdown for handheld LIBS

Metric	Weight	Score	Weighted
DP	0.30	7	2.1
PCC	0.20	4	0.8
M	0.10	9	0.9
OE	0.20	8	1.6
COI	0.20	8	1.6
TOTAL (GMTI)			**7.0**

4.2.2 Handheld XRF

4.2.2.1 Method description

This technique was tested in the initial stage of the project. Analyses were performed on the surface of raw ore samples and flake graphite concentrates without sample preparation. Two independent analyses were performed on each sample for a duration of 120 seconds by a Niton XL3t GOLDD+ (Thermo Scientific) instrument. At that stage of the project, it was not known, to which degree severe chemical within-sample heterogeneity stems from inhomogeneously distributed minerals, intermixed with graphite. The variance between individual measurements within the same sample exceeded between-deposit variance and resulted in the spuriously ubiquitous presence of Cd, Pd, Ag, Au, Nb and Bi in all samples. The analyses were therefore not conclusive and discontinued. Based on our current knowledge, a targeted analysis of pressed pellets, including a standard calibration series prepared for laboratory XRF measurements is expected to deliver more reliable results in the future.

Funded by
the European Union

5 Conclusion

This Deliverable D2.3 has established a robust and structured methodology for on-site material flow characterization within the framework of the MaDiTraCe project. Based on a harmonized comparative approach using five key criteria—mobility, production chain coverage, differentiating power, cost of implementation, and operational efficiency—the Global MFP Technic Index (GMTI) provides a relevant and practical tool to evaluate and select analytical techniques suited to traceability challenges.

The application of this methodology to the lithium and natural graphite value chains has demonstrated its relevance in different industrial contexts. For the lithium value chain, the work focused on identifying key leverage points for traceability along the production chain, from mineral concentrates to cathode active materials. Several on-site analytical techniques were tested and evaluated, including on-line LIBS, mobile µLIBS, portable and mobile XRF systems, as well as mineral luminescence-based methods (UV-bench and cathodoluminescence). The results demonstrate that geochemical signatures, particularly when processed using multivariate approaches and machine learning techniques, enable effective discrimination of material origins. The study also highlights the importance of controlling measurement-related effects (e.g. plasma conditions, matrix effects, sample preparation) and implementing appropriate calibration strategies to ensure robust performance under industrial conditions. For the natural graphite value chain, the study focused on the evaluation of portable techniques, mainly handheld LIBS, while only preliminary tests were conducted using handheld XRF, applied to graphite concentrates from various origins. The results show that LIBS captures significant variations in spectral signatures reflecting geological origin, with promising classification performance. However, certain limitations were identified, particularly regarding the detection of specific elements such as sulphur, underlining the need for complementary analytical approaches. XRF provides additional relevant information for selected trace elements, reinforcing the value of combined methodologies for traceability purposes. It should also be emphasized that, at the current stage of development, mobile analytical techniques are primarily applicable to the upstream part of the value chain (raw materials and concentrates). Their applicability to downstream stages (refined salts, active materials, or final products) remains limited due to analytical constraints, matrix transformations, and physicochemical changes occurring during processing. This highlights the need to develop or adapt complementary approaches to ensure continuity of traceability across the entire value chain. Overall, the results demonstrate that, despite certain limitations related to operational conditions and material variability, several on-site techniques show significant potential for discriminating material origin and supporting reliable traceability along the production chain. The central importance of differentiating power as a key criterion is reflected in the weighting strategy adopted in the GMTI, as well as in the overall methodology, alongside the relevance of integrated approaches combining data acquisition, advanced data processing, and calibration strategies. In this context, the results highlight the key role of on-site and on-line analytical techniques as a first tier for rapid anomaly detection along the production chain, enabling the timely identification of deviations and triggering a second tier of more detailed laboratory-based analyses when required (see D2.4). This two-level approach constitutes a central specificity of the methodology developed in D2.3, ensuring both operational efficiency and analytical reliability. Furthermore, the example of the Metso Courier® 8X SL on-line LIBS system demonstrates that existing industrial process control tools can be effectively adapted for traceability purposes, primarily through the implementation of

Funded by
the European Union

complementary data processing and interpretation strategies. This approach leverages already deployed analytical infrastructures, thereby significantly improving the cost–benefit balance of traceability systems

Finally, this work provides important perspectives for future developments beyond the project. Further investigations are required to extend the methodology to other critical raw materials (cobalt, neodymium), improve model robustness against measurement variability, and validate the proposed approaches under real industrial conditions and at larger scale. This methodology therefore provides a solid foundation for the development of integrated traceability systems, contributing to European objectives related to transparency, sustainability, and secure supply of critical raw materials.

Funded by
the European Union

Bibliography

Arató, R., Quarles, D., Obbágy, G., Dallos, Z., Arató, M., Gopon, P., & Melcher, F. (2025). Towards a chemical fingerprint of graphite by laser-induced breakdown spectroscopy. Journal of Analytical Atomic Spectrometry, 40(9), 2526–2537. https://doi.org/10.1039/d5ja00053j

Augustsson, C. & Reker, A. (2012). Cathodoluminescence Spectra of Quartz As Provenance Indicators Revisited. Journal of Sedimentary Research, 82(8), 559-570. doi: 10.2110/jsr.2012.51

Baele J.-M., Decrée, S., & Rusk, B. (2019). "Cathodoluminescence Applied to Ore Geology and Exploration" in Decrée S. and Robb L. Ore Deposits: Origin, Exploration, and Exploitation. doi: 10.1002/9781119290544.ch6

Brennan, C. J., Student, J. J., Hill, T., Martins, T., & Sirbescu, M.-L. C. (2024). Trace element concentrations and chemical zoning of spodumene from magmatic and hydrothermal origins. Ore Geology Reviews, 169, 106089. https://doi.org/10.1016/j.oregeorev.2024.106089

Cremers, D. A., & Radziemski, L. J. (2013). Handbook of laser-induced breakdown spectroscopy (2nd ed.). John Wiley & Sons.

Guezenoc, J., Gallet-Budynek, A., & Bousquet, B. (2019). Critical review and advices on spectral-based normalization methods for LIBS quantitative analysis. Spectrochimica Acta Part B: Atomic Spectroscopy, 160, 105688. https://doi.org/10.1016/j.sab.2019.105688

Kempe, U. & Götze, J. (2002). Cathodoluminescence (CL) behaviour and crystal chemistry of apatite from rare-metal deposits. Mineralogical Magazine, 66(1), 151-172. doi:10.1180/0026461026610019

Köresaar, L. (2016). Courier 8 SL Feasibility Test – Lithium application [Unpublished internal report]. Metso Oyj.

Liu , K., Sherwood, N., & Zhao, M. (2014). "Advances in Fluorescence Spectroscopy for Petroleum Geosciences" in Grice K. Principles and Practice of Analytical Techniques in Geosciences. pp 94-121. doi: 10.1039/9781782625025

Moradell-Casellas, A., Lohier, T., Laperche, V., Aupart, C., Bodereau, N., Desaulty, A.M. Better, faster, stronger: using handheld, mobile XRF instruments and statistical treatment to track on site the origin of lithium mineral concentrates. (in prep)

Reichl, C., & Schatz, M. (2025). World Mining Data 2025.